

PART I

THE STANDARD ENTROPIES OF SEVERAL COMPOUNDS

PART II

THEORY OF THE THERMAL DIFFUSION OF ELECTROLYTES IN A CLUSIUS COLUMN

PART III

A STUDY OF THE STRUCTURE OF SULFUR MONOCHLORIDE BY ELECTRON DIFFRACTION

PART IV

A STUDY OF FACTORS IN THE DESIGN AND USE OF AN ELECTRON DIFFRACTION CAMERA

Thesis by

George Boardman Guthrie, Jr.

In Partial Fulfillment of the Requirements

For the Degree of

Doctor of Philosophy

California Institute of Technology

Pasadena, California

1949

ACKNOWLEDGMENTS

This thesis would never have been completed without the help and encouragement of my many friends at the California Institute of Technology. I am indebted to my fellow graduate students for the mutual exchanges of ideas in "bull sessions" and to the members of the staff for instruction and individual discussions which have helped to clarify many fields of science.

I wish to express my appreciation to Dr. Hugh M. Huffman for my indoctrination into careful and precise experimentation and to thank Professor Leverett Davis for many discussions which he gave patiently and cheerfully. I am indebted to Dr. E. W. Hughes, Dr. Jurg Waser, and especially, Professor Verner Schomaker who have guided this research at its various stages and have made many helpful suggestions.

I am sincerely grateful for the opportunity which I have had to work in the Department of Chemistry. No one who has worked here can fail to appreciate the dynamic atmosphere created under the leadership of Professor Linus Pauling.

Finally, I wish to thank my wife, Margaret Sullivan Guthrie, who has patiently prepared the drawings and has typed this thesis.

ABSTRACT

The standard entropies of isopentane, ethyl benzene, azelaic acid and sebacic acid have been determined by the method of the third law of thermodynamics. An anomalous hysteresis in the heat capacity of isopentane reported by Aston et al. was not found. A transition was found in sebacic acid crystals and is discussed.

A theory is presented which accounts approximately for the apparently anomalous difference between the thermal diffusion coefficients of the ions of an electrolyte in the presence and in the absence of other electrolytes.

The structure of sulfur monochloride has been redetermined by electron diffraction. The molecule was found to have an extended structure. The parameters have been determined and are reported.

The theoretical expression for the scattering of electrons by gases is altered by a camera of finite dimensions. An approximate theory of the alteration in terms of the camera dimensions (and electron lens parameters) has been developed. An expression for the effect of multiple scattering has been obtained.

TABLE OF CONTENTS

PART	PAGE
I	The Standard Entropies of Several Compounds 11
	Isopentane (reprint) 11
	Ethylbenzene (reprint) 66
	Azelaic and Sebacic Acids 8
	References 24
II	Theory of the Thermal Diffusion of Electrolytes in a Clusius
	Column 255
	References 37
III	A Study of the Structure of Sulfur Monochloride by Electron
	Diffraction 38
	References 50
IV	A Study of Factors in the Design and Use of an Electron
	Diffraction Camera 51
	Table of Contents 52
	Appendix 107
	References 108
	Propositions 109

PART I

THE STANDARD ENTROPIES OF SEVERAL COMPOUNDS

ISOPENTANE

ETHYLBENZENE

AZELAIC ACID AND SEBACIC ACID

[CONTRIBUTION FROM THE WILLIAM G. KERCKHOFF LABORATORIES OF THE BIOLOGICAL SCIENCES, CALIFORNIA INSTITUTE OF TECHNOLOGY]

Thermal Data. XVI. The Heat Capacity and Entropy of Isopentane. The Absence of a Reported Anomaly

BY GEORGE B. GUTHRIE, JR., AND HUGH M. HUFFMAN

In two recent papers¹ Aston and co-workers have reported the results of their low temperature studies on isopentane. During this investigation they obtained certain anomalous results in their heat capacity and vapor pressure measurements. These anomalous results were especially evident in the temperature interval 180 to 240°K. Aston has attempted to account for these results on the basis of a hysteresis in the establishment of equilibrium between isomeric forms due to hindered rotation. The heat capacity of isopentane was also measured in 1930 by Parks, Huffman and Thomas,² who did not observe any irregularities in the heat capacity.

Because of the great importance of such a phenomenon and the great effect its existence would have upon similar experimental and theoretical studies on other hydrocarbon molecules, it is of paramount importance that its actual existence be established beyond any reasonable doubt.

We have accordingly reinvestigated the heat capacity of isopentane over the temperature range 13 to 300°K. Unfortunately, the design of our apparatus did not permit the simultaneous observation of the vapor pressure.

(1) (a) Aston and Schumann, *THIS JOURNAL*, **64**, 1034 (1942);
(b) Schumann, Aston and Sagenkahn, *ibid.*, **64**, 1039 (1942).

(2) Parks, Huffman and Thomas, *ibid.*, **62**, 1032 (1930).

Experimental

The Material.—Measurements were made on two different samples of isopentane. The first was purified for us by the Shell Development Company, who state that the entire sample, 300 cc., boiled at $27.92 \pm 0.01^\circ\text{C}$. The second sample was the isopentane that Aston, *et al.*,¹ had used in their calorimeter and was kindly sent to us by Professor Aston. From data obtained during the melting point determinations we have calculated that the liquid-soluble, solid-insoluble impurity in the first (Shell) sample was 0.013 mole per cent. and that in the second (Aston) sample was 0.008 mole per cent.

The Apparatus.—Our heat capacity measurements were carried out in an adiabatic calorimetric system which will be described in detail in a later publication. The calorimeter proper was of copper and had an internal volume of approximately 60 cc.

The isopentane was transferred to the calorimeter by distillation through a glass system to which the calorimeter was connected by a glass to metal seal. This system was connected to the high vacuum line and to the source of helium by means of stopcocks, which were greased with Apiezon grease M. The stopcocks were so placed as to be out of the direct distillation path. In transferring the first sample (Shell) to the calorimeter it was necessary to expose the isopentane to the air for a short time hence precautions were taken to remove any water, which might have gotten into the sample, by several distillations from phosphorus pentoxide in the closed system. The second sample (Aston) was received in a container that could be sealed directly into the transfer system before opening. In both cases the system and the sample were carefully outgassed by pumping with an oil diffusion pump while the isopentane was frozen in liquid air. After outgassing the

calorimeter was immersed in a bath of solid carbon dioxide and alcohol and the isopentane distilled in. When the transfer was completed helium was admitted and the system allowed to warm to room temperature. The monel metal filling tube, 1.0 mm. o. d., was then pinched off close to the calorimeter and quickly made gas tight by the application of a small drop of soft solder. The pressure of helium in the calorimeter was approximately 40 mm. at room temperature. In the first case (Shell sample) the amount of isopentane in the calorimeter was 35.598 g. (0.49341 mole) and the gas space at 300°K. was 2.28 cc. In the second case the amount of isopentane in the calorimeter was 24.884 g. (0.34491 mole) and the gas space at 300°K. was 10.67 cc. This undesirably large gas space was due to the limited amount of material that was available.

It is of considerable importance to note that after the isopentane was sealed into the calorimeter there was no chance for it to be transferred to any other part of the calorimetric system, hence the mass of the isopentane upon which observations were made was constant.

Temperature measurements were made with a platinum resistance thermometer, H-8, which had been compared against the laboratory standard platinum thermometer, H-25, which in turn had been calibrated by the Bureau of Standards over the temperature range 14°K. to the boiling point of sulfur. The energy measurements were made in terms of the international joule by utilizing resistors and standard cells which had been compared with others certified by the Bureau of Standards. The observed energies in international joules were converted to calories by dividing by 4.1833.

TABLE I
MOLAL HEAT CAPACITY OF ISOPENTANE, ARRANGED CHRONOLOGICALLY
Molecular weight = 72.146, 0°C. = 273.16°K.

T, °K.	C _p , cal./degree	T, °K.	C _p , cal./degree	T, °K.	C _p , cal./degree	T, °K.	C _p , cal./degree	T, °K.	C _p , cal./degree
Series I, solid		Series IV, liquid		Series X, liquid		Series XVIII, solid		Series XXII, liquid	
84.78	16.07	115.67	29.48	188.13	32.40	13.20	1.119	214.82	33.730
87.69	16.57	122.87	29.76	197.01	32.81	14.61	1.482	224.23	34.229
90.97	17.13	133.94	30.19	206.76	33.29	16.42	1.956	233.50	34.798
94.58	17.78	149.26	30.79	216.34	33.80	19.20	2.750	242.41	35.360
98.08	18.42	159.80	31.19	225.78	34.31	22.90	3.861	251.39	35.940
101.44	19.11	170.16	31.63	235.08	34.86	26.94	5.034	260.23	36.569
104.70	19.77	180.35	32.05	Series XI, solid		31.92	6.390	268.92	37.192
107.85	20.44	190.38	32.51	67.21	14.01	37.65	7.821	277.49	37.804
110.94	21.23	200.25	32.98	69.46	14.67	43.41	9.072	285.92	38.445
Liquid		Series V, liquid		Series XII, solid		49.20	10.24	294.21	39.132
120.05	29.67	171.33	31.66	Series XIII, solid		55.03	11.38	Series XXII, solid	
124.44	29.84	181.50	32.09	71.46	15.30	Series XIX, solid		55.40	11.461
Series II, solid		191.51	32.54	Series XIV, liquid		15.75	1.814	59.98	12.371
58.74	12.11	201.36	33.02	52.92	10.95	18.62	2.590	64.65	13.389
62.08	12.82	211.05	33.51	56.98	11.77	22.51	3.745	67.72	14.076
65.22	13.52	220.60	34.02	Series XV, liquid		27.10	5.083	69.37	14.639
68.19	14.29	230.00	34.56	188.66	32.42	32.17	6.424	70.96	15.294
70.99	15.19	239.26	35.12	198.50	32.87	37.98	7.894	72.51	15.456
71.33	15.60	248.37	35.69	208.18	33.36	44.20	9.238	74.07	14.552
Series III, solid		257.34	36.29	208.18	33.36	49.50	10.29	76.25	14.743
54.79	11.30	267.90	37.08	217.70	33.87	Series XX, liquid		78.98	15.155
58.59	12.06	Series VI, liquid		227.08	34.39	184.29	32.220	83.19	15.822
62.59	12.91	209.78	33.43	Series XVII, liquid		194.20	32.664	89.41	15.897
66.31	13.77	219.34	33.95	189.41	32.46	203.97	33.165	95.89	18.031
69.24	14.54	Series VII, liquid		199.25	32.94	213.57	33.667	101.96	19.220
71.44	15.52	184.60	32.22	208.93	33.41	223.04	34.165	107.41	20.385
73.58	15.11	Series VIII, liquid		219.40	33.97	232.35	34.757	111.24	21.716
76.01	14.79	230.62	34.61	Series XVIII, liquid		241.52	35.293	Liquid	
78.95	15.14	231.34	34.65	230.62	34.61	250.54	35.899	115.86	29.495
82.56	15.71	Series IX, liquid		Series XIX, liquid		275.42	36.496	122.84	29.761
86.47	16.37	186.49	32.33	253.56	36.04	Series XXI, liquid		132.77	30.138
90.52	17.08	192.67	32.60	262.79	36.69	187.58	32.400	143.53	30.550
95.44	17.94			271.88	37.38	197.45	32.858	154.11	30.968
101.42	19.10			280.38	38.00	207.16	33.328	164.49	31.394
107.68	20.51			288.76	38.62	216.71	33.844	174.69	31.814
				297.00	39.28	226.12	34.380		
				Series XVII, liquid		235.38	34.919		
				297.81	39.31				

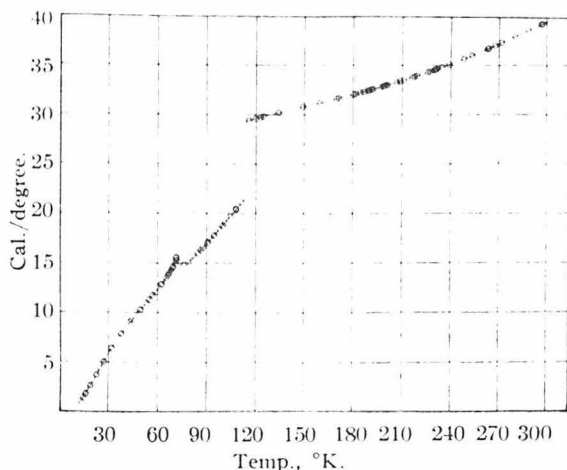


Fig. 1.—The molal heat capacity of isopentane.

The Heat Capacity.—The results of our heat capacity determinations on both samples are given in Table I and those on sample one are shown graphically in Fig. 1. The results of the heat capacity measurements on the two samples of isopentane are in complete agreement in the temperature ranges investigated. For this reason we did not feel that it was necessary to extend our measurements on the second sample (Aston) below 53°K. In view of the nature of our problem we have reported the results of each experimental series of observations as a group (Table I). In Fig. 2 we have presented graphically the (time-temperature) history of our first (Shell) sample. By reference to Fig. 2 and Table I a knowledge of the treatment of the sample preceding each series of measurements may be obtained. The time-temperature history of the second sample (Aston) is not shown on this curve. However in the temperature region 180–240°K. it was given a fast and slow cooling treatment similar to that shown for the first sample.

In the temperature region 180–240°K. repeated attempts were made to obtain evidence of an anomalous behavior. During the early part of this investigation we corresponded with Aston and asked him to suggest an experimental procedure which would cause this phenomenon to manifest itself. In reply he wrote, "We suggest that you cool across the vacuum from 290 to 180°K. in thirty-six hours (Series I), and warming to 290°K. again cool from this temperature to 180°K. in not more than four hours (Series II). In each case take measurements from 180 to 230°K. This procedure should produce a difference in heat capacity of at least 1%, Series I

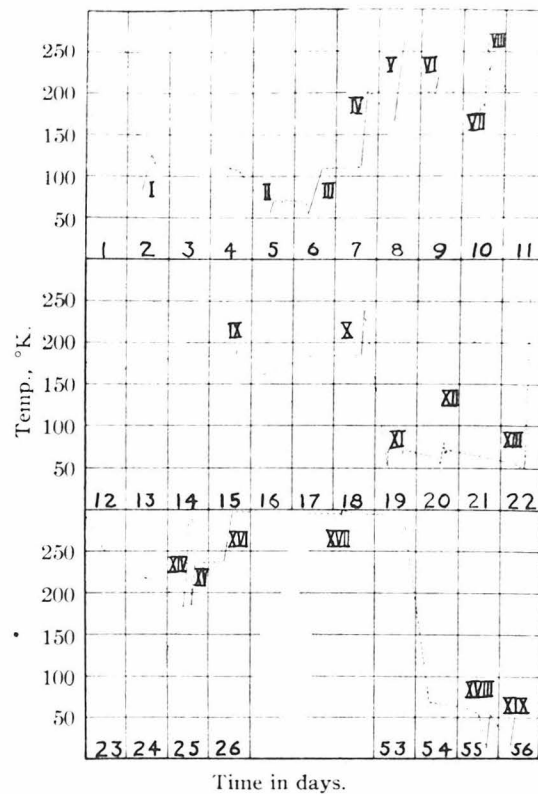


Fig. 2.—Time-temperature history of isopentane: solid lines ascending to right indicate heat capacity measurements, Series I–XIX consecutively. Dashed lines indicate temperature of the isopentane in the intervals between heat capacity measurements. Break in lower section of graph indicates a period of 27 days when isopentane was at room temperature.

being higher than Series II." We carried out experiments according to these directions (our Series XIV and XV on the Shell sample and Series XX and XXI on Aston sample) except that our slow cooling required a longer time and our fast cooling was done more rapidly than suggested. The results of all of our experiments yield heat capacities that lie on a perfectly smooth curve within the precision of our measurements which is approximately 0.1% (deviation) in the region in question.

The Heat of Fusion.—Two measurements of the heat of fusion were made on the Shell sample, one of which was in conjunction with the melting point determination. The value obtained for the heat of fusion was 1232.2 cal./mole with an estimated uncertainty of less than 1 calorie. A single value of the heat of fusion of sample two (Aston) was calculated from data obtained during the melting point determination. The value of the heat of fusion found was 1229.2 calories per

mole. This value is about 0.2% lower than the value found for the first sample and is probably less reliable due to the experimental method.

We have calculated the melting point of pure isopentane from data obtained when various fractions of the two samples were melted. The first sample (Shell) gave a melting point of 113.371°K. and the second (Aston) 113.368°K. from which we conclude that the melting point of pure isopentane is $113.37 \pm 0.05^\circ\text{K}$. This is in excellent agreement with Aston's value $113.39 \pm 0.05^\circ\text{K}$.

The Entropy.—We have also calculated the entropy of isopentane from our data. The results of these calculations are summarized in Table III.

Discussion

Aston's plot of his experimental data indicates an anomalous behavior especially in the temperature intervals 20–60°K. and 180–240°K. Our measurements in both of these temperature regions show no anomalous results. In cooling the isopentane through the 70° transition zone we cooled both rapidly and slowly. The measurements in Series II were made after rapid cooling, all of the other measurements below 73°K., with one exception, were made after the isopentane had been allowed to cool slowly, approximately 0.4–0.5° per hour, in the region 71 to 60°K. The single measurement in Series XII was made after cooling rapidly (twenty-five minutes) from 80.4 to 69.8°K. in an attempt to get a point on an extrapolation of the high temperature curve as we have been able to do in the case of a similar transition found in sebacic acid (unpublished investigation). The attempt was unsuccessful. Below 69°K. all of the experimental results were in complete agreement. In the region 69 to 77°K. the points did not lie on any regular curve; this may be due to the fact that the temperature increments were too large and that they did not cover the same portion of the temperature scale or to the fact that the energy absorption in this region is a function of the history of the sample. The measurements on sample two (Aston) in this region gave approximately the same temperature (72°) for the maximum energy absorption but the total energy absorbed is definitely lower than in the case of sample one.

Aston made four series of measurements on the solid at liquid hydrogen temperatures and found

evidence for hysteresis. We made two series of measurements between 13 and 55°K. and several additional series of measurements between 53 and 70°K. without finding any evidence of an anomalous behavior. We are unable to compare our data with Aston's experimental points since he has only published the values taken from a smoothed curve. However, we submitted our data to Aston prior to publication and in a communication to Dr. A. B. Lamb he states that his low curve between 10 and 55°K. is essentially in agreement with our curve.

In the temperature region 180–240°K. our re-

TABLE II
MOLAL HEAT CAPACITY OF ISOPENTANE AT ROUNDED TEMPERATURES

T, °K.	C _p , cal./degree		% diff. from H and G			
	H. and G.	A. and S.	S ₁	P ₁	S ₂	H and T.
Crystals						
13	1.07					
15	1.58					
20	3.00	3.25			8.3	
25	4.49	4.82			7.3	
30	5.86	6.00			2.4	
35	7.18	7.24			0.8	
40	8.34	8.41			.8	
45	9.40	9.46			.6	
50	10.39	10.41			.2	
55	11.38	11.36			-.2	
60	12.37	12.38			.1	
70	(14.8) ^b	15.00				
80	15.24	15.19	15.58		-.3	-.2
90	16.99	16.96	17.14		-.2	-.9
100	18.79	18.81	19.54		.1	1.0
110	20.99	20.75			-1.0	
Liquid						
115	29.46					
120	29.66	29.68	29.55	0.07		-.37
130	30.04	29.99	29.95	-.17		-.30
140	30.42	30.38	30.34	-.13		-.26
150	30.80	30.72	30.74	-.26		-.20
160	31.20	31.06	31.14	-.45		-.19
170	31.61	31.48	31.55	-.41		-.19
180	32.04	31.95	32.00	-.28		-.10
190	32.48		32.46			-.06
200	32.96		33.00			-.12
210	33.46		33.50			-.12
220	34.00		34.04			-.12
230	34.58		34.60			-.09
240	35.18	35.20	35.20	.06		.06
250	35.82	35.89	35.80	.20		-.06
260	36.52	36.59	36.48	.19		-.11
270	37.24	37.37	37.10	.35		-.38
280	37.98	38.31	37.75 ^a	.87		-.61
290	38.75	40.49 ^a		4.49		
300	39.55					

^a Extrapolated values. ^b In transition zone, actual value not certain.

sults show no evidence of an anomalous behavior in either of the two samples that we have studied. These results lead us to the belief that the hysteresis in the liquid observed by Aston is not characteristic of isopentane. We have sent Aston a portion of the Shell isopentane upon which he will repeat his measurements.

Another noteworthy result of this reinvestigation of the heat capacity of isopentane is the lack of agreement between our results and those of Aston, even in the temperature regions in which Aston reports no anomalous results. In Table II we have compared the data taken from a smooth curve through our data with those from Aston's smoothed table. For sake of completeness we have also included the data of Parks, Huffman and Thomas. The accuracy (1%) claimed by the latter authors is not high, neither did they make any estimate of the impurity in their sample, so little weight should be given to the apparent discrepancies between their results and those of the other two investigations.

TABLE III

THE MOLAL ENTROPY OF ISOPENTANE

S (13.21, Debye, 6° freedom)	$= 0.385 \pm 0.040$
ΔS (13.21 - 113.37)	$= 19.174 \pm .019$
ΔS (113.37, fusion)	$= 10.869 \pm .011$
ΔS (113.37 - 298.16)	$= 31.812 \pm .032$
S (298.16, liquid)	$= 62.240 \pm .10$

An examination of the data in Table II shows that at 20°K. Aston's results are about 8% higher than those of this investigation; this difference becomes progressively less as the temperature is increased. From 55 to 100°K. the heat capacity measurements are essentially in agreement. Above the melting point the discrepancies range from

-0.45 at 160°K. to 4.5% at 290°K. The above discrepancies are of such a magnitude as to suggest that the accuracy claimed in one or the other or both of these investigations is entirely fictitious. This suggests that perhaps the accuracy claimed by other laboratories may be open to question.

We should like to propose that workers in this field select a substance whose heat capacity has been accurately determined which may be used as a standard test substance.

The discrepancies in the experimental observations have very little effect on the agreement of the values of the entropies calculated from the two sets of data. Our value for the entropy of liquid isopentane at 298.16°K. is only 0.15 unit lower than that reported by Aston, which is well within the error assigned by him.

Summary

1. The heat capacity of isopentane has been measured over the temperature range 13 to 300°K.
2. The melting point and heat of fusion of isopentane have been measured.
3. We believe that the results of this investigation indicate that certain anomalous results reported by Aston are not characteristic of isopentane.
4. The entropy of liquid isopentane at 298.16°K., calculated from the data of this research, is 62.24 ± 0.10 cal. degree⁻¹ mole⁻¹.
5. It is suggested that thermochemists should check their methods so that the accuracy assigned to the experimental results will have a real significance.

PASADENA, CALIFORNIA

RECEIVED JANUARY 16, 1943

[CONTRIBUTION FROM THE WILLIAM G. KERCKHOFF LABORATORIES OF THE BIOLOGICAL SCIENCES, CALIFORNIA INSTITUTE OF TECHNOLOGY]

Thermal Data. XVIII. The Heat Capacity, Heat of Fusion, Entropy and Free Energy of Ethylbenzene

BY GEORGE B. GUTHRIE, JR., RALPH W. SPITZER AND HUGH M. HUFFMAN¹

Some time ago this Laboratory began a research program involving the study of certain thermal properties of hydrocarbons. Because of the importance of ethylbenzene in hydrocarbon chemistry a study was made of its low temperature thermal properties. In this paper we present the results of this investigation. These data have been utilized to calculate the entropy and free energy of liquid ethylbenzene at 298.16°K.

The Ethylbenzene.—The material used in this investigation was supplied to us in the purified condition by the Shell Development Co. An estimate of the liquid soluble–solid insoluble impurity was made from data obtained by observing the equilibrium temperatures corresponding to known fractions of the material in the solid and liquid form. The impurity estimated from the above data was 0.070 mole per cent.

Experimental. The experimental method has been described in a recent paper by Ruchwein and Huffman² and only a brief description need be given here. An adiabatic calorimetric system was used in which the material under investigation was contained in a sealed copper calorimeter. A measured quantity of electrical energy was supplied to the calorimeter and at all times during the measurements the temperature of the environment was maintained at that of the calorimeter to prevent heat interchange. The initial and final temperatures of the calorimeter were measured by means of a platinum resistance thermometer. The electrical measurements required for the determination of the energy and of the resistance of the thermometer were made on a White double potentiometer in conjunction with a high sensitivity galvanometer and accurately calibrated resistances. The precision of our measurements is in general better than 0.1% and we believe that above 30°K. the accuracy should be about the same as the precision. The energy measurements were made in terms of the international joule and were converted to the conventional calorie by dividing by 4.1833.

The ethylbenzene was distilled into the calorimeter in an air-free system. The gas space was filled with helium at one atmosphere pressure at room temperature and the calorimeter was then sealed by the application of a drop of soft solder.

The results of the heat capacity measurements are given in Table I. Most of the temperature range was covered at least twice and the results of the measurements in the different series were in excellent agreement. In Table II we have listed the values of the heat capacity at integral temperatures as selected from a smooth curve through all of the data.

(1) Present address, Bureau of Mines, Bartlesville, Oklahoma.

(2) Ruchwein and Huffman, THIS JOURNAL, 65, 1620 (1943).

TABLE I
MOLAL HEAT CAPACITY OF ETHYLBENZENE
Molecular weight = 106.160; 0°C. = 273.16°K.

T_M , °K.	ΔT	C_p cal./degree	T , °K.	ΔT	C_p , cal./de- gree
		Crystals	109.43	6.235	17.960
13.34	1.351	1.013	115.01	16.868	18.604
15.01	1.973	1.380	116.53	7.950	18.749
16.91	1.831	1.846	126.79	12.578	19.859
19.72	4.067	2.585	133.33	19.762	20.629
19.84	4.030	2.638	138.98	11.814	21.222
23.90	4.098	3.809	150.47	11.167	22.482
24.09	4.676	3.859	154.21	22.013	22.952
27.99	4.080	4.965	160.62	9.130	23.677
28.40	3.946	5.086	166.84	3.244	24.622 ^a
32.28	4.493	6.150	170.04	3.158	25.464 ^a
32.97	5.186	6.333	173.13	3.022	26.926 ^a
37.07	5.085	7.374			Liquid
38.59	4.217	7.728	181.51	9.249	37.648
42.06	4.889	8.513	190.70	9.152	37.936
46.39	9.538	9.375	199.81	9.056	38.257
47.14	5.288	9.524	208.81	8.954	38.626
52.28	4.994	10.480	216.27	9.601	38.982
55.96	9.605	11.120	218.15	9.733	39.048
57.76	5.971	11.436	221.14	17.426	39.211
62.40	3.916	12.177	225.80	9.473	39.446
63.91	6.284	12.410	234.98	10.249	39.989
66.21	3.696	12.755	244.70	10.074	40.532
71.14	6.165	13.445	255.52	11.553	41.246
77.09	5.741	14.272	266.96	11.346	42.016
83.19	6.452	15.028	277.41	9.556	42.787
89.95	7.063	15.874	286.89	9.406	43.504
96.82	6.692	16.617	296.23	9.254	44.275
103.37	6.413	17.318	305.41	9.113	44.994
103.43	5.766	17.320			

^a These values include premelting.

The Melting Point.—In Table III we have given the equilibrium temperatures corresponding to the known fraction of calorimeter contents in the liquid state.³ Utilizing these data we have calculated the melting point of the mixture in the calorimeter and also for pure ethylbenzene. The values of the melting point given in the last column of Table III were calculated, by an approximate method, on basis of an impurity of 0.070 mole per cent. From these data we conclude that the melting point

(3) The value given as per cent. liquid is actually the per cent. of the calculated heat of fusion of the contents of the calorimeter but for practical purposes this may be taken as representing the per cent. of the ethylbenzene in the liquid form.

TABLE II
MOLAL HEAT CAPACITY OF ETHYLBENZENE AT INTEGRAL
TEMPERATURES

T, °K.	C_p , cal./degree	T, °K.	C_p , cal./degree
Crystals			
13	0.94	130	20.23
15	1.39	150	22.47
20	2.68	160	23.61
25	4.12	170	24.75
30	5.53	175	25.32 ^a
35	6.85	Liquid	
40	8.06	180	37.61
45	9.11	190	37.91
50	10.06	200	38.26
55	10.96	210	38.68
60	11.80	220	39.16
65	12.57	230	39.68
70	13.30	240	40.25
75	13.99	250	40.88
80	14.64	260	41.54
85	15.26	270	42.24
90	15.86	280	42.98
100	16.96	290	43.76
110	18.04	300	44.56
120	19.14		

^a Extrapolated.

of pure ethylbenzene is $178.17 \pm 0.03^\circ\text{K}$. We wish to point out that the observed value for the melting point when 5.7% of the ethylbenzene was liquid is not in agreement with the calculated value. This may be taken as indicating a deviation from the laws of the ideal dilute solution.

TABLE III
MELTING POINT SUMMARY

% Melted	Obs. m. p., °K.	M. p., °C. (calcd.) ^a
5.7	177.880	177.814
25.0	178.090	178.090
45.4	178.122	178.124
75.5	178.142	178.142
93.5	178.147	178.147
100.0	(178.149)	178.149
Pure	$178.169 \pm 0.03^\circ$	

^a These values calculated on the basis that the solid insoluble-liquid soluble impurity is 0.070 mole per cent.

We have also determined the heat of fusion of ethylbenzene and the results of two determinations of this quantity are given in Table IV. It is to be noted that this quantity is somewhat arbitrary since it is impossible to uniquely

TABLE IV
FUSION DATA SUMMARY

Fusion	Cal./mole	Dev.
1	2189.1	-1.2
2	2191.5	+1.2
Mean	2190.3	

determine the true heat capacity curve in the region below the melting point. This uncertainty in the heat of fusion will have only a minor effect on the entropy calculated from these data.

We have also calculated the entropy of liquid ethylbenzene at 298.16°K . The results of these calculations are summarized in Table V. The entropy of ethylbenzene

TABLE V

THERMAL DATA FOR ETHYLBENZENE, SUMMARY ENTROPY

$S(0-14^\circ) = 0.3984$ (Debye 6° freedom, $\theta = 128$)
 $\Delta S(14.0-178.17) = 27.604$ graphical
 $\Delta S(\text{fusion}, 178.17) = 12.293$
 $\Delta S(178.17-298.16) = 20.654$
 $S(\text{Liquid } 298.16) = 60.95 \pm 0.10$ cal. degree⁻¹ mole⁻¹

was also calculated by Huffman, Parks and Daniels⁴ from the results of their low temperature measurements which extended only down to 90°K . They obtained a value of 61.2 E. U./mole in excellent agreement with our more accurate value of 60.95 E. U./mole. Prosen and Rossini have recently determined the heat of combustion of ethylbenzene and give the value $\Delta H_R^\circ = -1091.03$ kcal./mole.⁵ This datum has been utilized in conjunction with the entropy reported in this paper and other data to calculate the free energy of formation of liquid ethylbenzene. The data are summarized in Table VI. In

TABLE VI

THE MOLAL FREE ENERGY OF FORMATION OF LIQUID
ETHYLBENZENE AT 298.16°K .

Heat of comb., ΔH° , kcal.	ΔH_f° , kcal.	ΔS , cal./degree	ΔF_f° , kcal.
-1091.03	-2.98	-106.08	28.65

making this calculation we have used the values 1.36⁶ and 31.23⁷ E. U. for the entropies of graphitic carbon and hydrogen gas, respectively, and the values 68318.1⁸ and 94,052⁹ calories for the molal heats of formation at 25° of liquid water and gaseous carbon dioxide, respectively.

In conclusion we wish to express our thanks to the Shell Development Co. for supplying the sample of ethylbenzene and also for financial assistance which made this investigation possible.

Summary

The heat capacity, heat of fusion and melting point of ethylbenzene have been measured.

The molal entropy and free energy of formation of liquid ethylbenzene at 298.16°K . have been calculated, $S = 60.95$ cal./degree and $\Delta F_f^\circ = 28.65$ kcal.

BARTLESVILLE, OKLA.

RECEIVED AUGUST 31, 1944

- (4) Huffman, Parks and Daniels, *THIS JOURNAL*, **52**, 1547 (1930).
 (5) Prosen and Rossini, private communication, to be published in *J. Research Nat. Bur. Standards*.
 (6) Jacobs and Parks, *THIS JOURNAL*, **56**, 1513 (1934).
 (7) Giauque, *ibid.*, **52**, 4816 (1930).
 (8) F. D. Rossini, *Bur. Standards J. Research*, **22**, 407 (1939).
 (9) Prosen and Jessup and Rossini, private communication, to be published in *J. Research Natl. Bur. Standards*.

THE HEAT CAPACITIES AND ENTROPIES
OF AZELAIC AND SEBACIC ACIDS *

The statistical mechanics of the solid state can treat only the very simplest solids; hence, empirical methods, such as those of Parks and Huffman¹, offer the most fruitful approach to the estimation of the thermodynamic properties of organic solids. The determination of the energy relations in the homologous series of dicarboxylic acids will be of great value in such empirical estimations since all the members of this series are solids at 25°C. It will be interesting also to learn whether or not these properties show alternations similar to those in the melting points and other physical properties. Furthermore, this class of organic compounds seems to have been neglected in the determination of thermodynamic data².

In 1942 the authors started on such a study of this series. When the calorimetric laboratory was dismantled and moved to the Petroleum Experiment Station of the Bureau of Mines, only the determination of the heat capacities and entropies of azelaic acid, $\text{HOOC}(\text{CH}_2)_7\text{COOH}$, and of sebacic acid, $\text{HOOC}(\text{CH}_2)_8\text{COOH}$, had been completed. Since there is little prospect that either of the authors will resume this investigation in the near future, the results which were obtained are reported in this paper.

Experimental

The Materials. -- Both the azelaic and sebacic acids used in this

* This research was conducted with Dr. H. M. Huffman, at that time assistant professor in the Wm. G. Kerckhoff Laboratories of the Biological Sciences.

study were obtained from the Eastman Company and were of White Label quality. These products were recrystallized several times from hot water and dried in an oven at 90°C . Uncorrected melting points found in a Hirschberg apparatus were 105.5 - 106.5°C . for azelaic acid and 130 - 131.5°C . for sebacic acid. The melting points given in the literature are 106.5°C . and 134.5°C . respectively.

The Apparatus and Experimental Method.— The measurements were made in the apparatus and by the procedure which is described in detail by Ruehrwein and Huffman³. Only a brief outline will be given here.

A copper calorimeter filled with about forty grams of the material under study was mounted in an adiabatic calorimetric system in which the temperature of the environment was maintained at the temperature of the surface of the calorimeter to minimize heat interchange at all times during observations. For each of the experimental heat capacities reported a measured amount of electrical energy was transferred to the calorimeter by means of a manganin resistance heater, and the initial and final temperatures were measured by means of a platinum resistance thermometer. The average heat capacity of the substance was calculated from the data after making corrections which included the heat capacity of the calorimeter vessel and the thermometer.

The electrical measurements required for the determination of the electrical energy and of the resistance of the platinum thermometer were made on a White double potentiometer in conjunction with a high sensitivity galvanometer and accurately calibrated resistances. The potential was in terms of an Eppley unsaturated cell which had been compared with others certified by the Bureau of Standards. Time was measured by means

of an electric stop clock driven by power from Boulder Dam. The electric timer was compared occasionally with a calibrated stop watch. The agreement between the two timers was always 0.1 sec. or better. The precision of the measurements was in general better than 0.1%; above 30°K. it is believed that the absolute uncertainty of the measurements is not greater than 0.2%. The energy measurements were made in terms of the international joule and were converted to calories by dividing by 4.1833.

Procedure for Filling the Solid Calorimeter. -- The paper of Ruehrwein and Huffman⁵ described the use of the cryostat and calorimeter with liquids only. Some of the calorimeters used in this apparatus may be used for either solids or liquids. One of these calorimeters was disassembled and filled with layers of solid interspersed with thin copper disks. When the calorimeter was full the lid was resoldered. With materials whose melting points are as high as those used in this investigation, this operation may be performed quickly enough to prevent melting the solid. The calorimeter was then connected to the vacuum bench by means of the filling tube and the air pumped out. A fraction of an atmosphere of helium was admitted and the filling tube sealed with a drop of solder. The helium speeds the attainment of thermal equilibrium within the calorimeter.

Results

The experimental heat capacities of azelaic and sebacic acids are given in Table I and are plotted in Figure 1. In Table II are listed the values of the molal heat capacity of both compounds at integral temperatures as selected from a smoothed curve drawn through the experimental data. The heat capacity data have been used to calculate the entropy of

TABLE I

MOLAL HEAT CAPACITIES

$0^{\circ}\text{C.} = 273.16^{\circ}\text{K.}$

Azelaic Acid

Molecular weight = 188.218

$T_M, ^{\circ}\text{K.}$	ΔT	C_p cal./degree	$T_M, ^{\circ}\text{K.}$	ΔT	C_p cal./degree
13.55	2.227	1.207	90.09	5.963	26.500
13.76	2.139	1.262	90.62	7.441	26.588
15.79	2.252	1.774	97.84	6.999	28.122
16.50	3.340	1.986	105.47	8.256	29.798
18.23	2.632	2.502	114.27	9.330	31.402
20.22	4.100	3.160	123.35	8.840	33.116
21.05	2.999	3.451	131.99	8.448	34.655
24.65	4.219	4.782	140.28	8.118	36.138
25.26	5.971	5.026	149.95	11.221	37.769
29.02	4.502	6.478	160.93	10.737	39.598
31.44	6.392	7.477	171.46	10.327	41.326
33.53	4.531	8.334	181.58	9.961	42.989
37.70	6.167	10.044	191.38	9.642	44.616
39.16	6.747	10.615	200.88	9.353	46.205
44.67	7.777	12.762	206.87	7.658	47.196
45.56	6.043	13.103	215.18	8.960	48.596
51.13	5.096	15.157	224.74	10.156	50.278
51.70	6.265	15.356	235.55	11.475	52.329
54.06	3.533	16.176	246.84	11.101	54.401
56.46	5.564	17.033	257.77	10.750	56.511
58.48	5.310	17.687	268.36	10.426	58.603
64.48	6.695	19.649	278.63	10.132	60.621
70.85	6.036	21.474	287.81	8.208	62.593
77.31	6.891	23.238	295.92	8.013	64.417
82.88	8.056	24.727	303.85	7.835	66.135
83.94	6.356	25.008			

Sebacic Acid

Molecular weight = 202.244

Stable crystals					
			146.52	1.943	44.063
			148.43	9.499	43.290
13.93	3.023	1.561	148.80	2.607	43.498
14.00	1.987	1.583	151.43	2.658	42.101
16.36	2.746	2.254	154.09	2.647	42.171
17.02	3.136	2.457	158.84	11.331	42.965

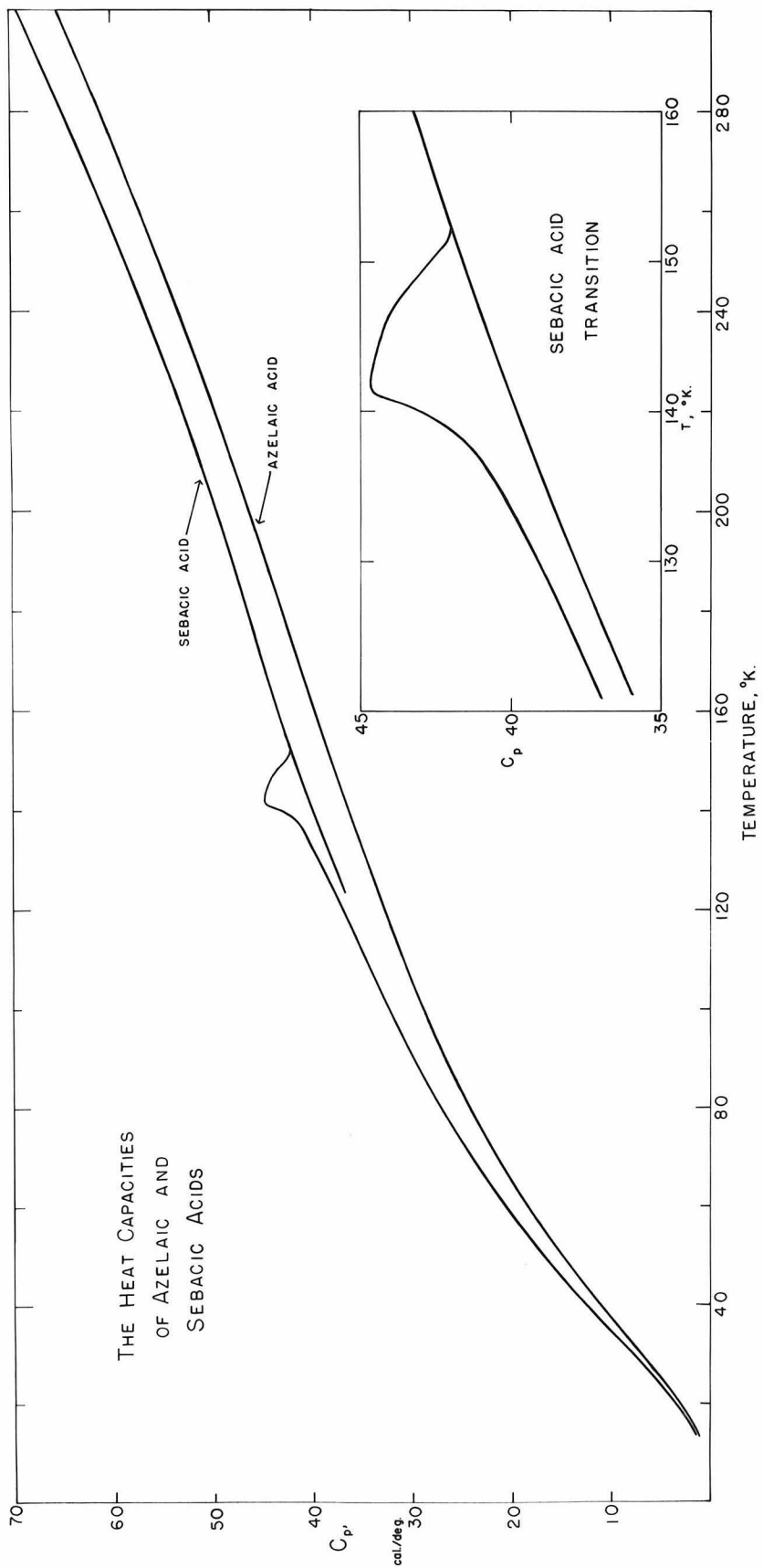


FIGURE 1

TABLE II

MOLAL HEAT CAPACITIES AT ROUNDED TEMPERATURES

$0^{\circ}\text{C.} = 273.16^{\circ}\text{K.}$

T, °K.	C_p cal./degree	
	Azelaic Acid M.W. = 188.218	Sebacic Acid M.W. = 202.244
15	1.59	1.86
20	3.09	3.51
25	4.93	5.56
30	6.87	7.77
40	10.95	12.37
50	14.75	16.72
60	18.21	20.56
70	21.24	23.95
80	23.97	27.01
90	26.47	29.69
100	28.58	32.10
110	30.59	34.39
120	32.51	36.71
130	34.33	39.09
140	36.10	43.3
150	37.78	43.0
160	39.47	43.17
170	41.36	44.72
180	42.73	46.22
190	44.38	47.66
200	46.06	49.84
210	47.74	50.83
220	49.45	52.59
230	51.28	54.44
240	53.18	56.36
250	55.02	58.37
260	56.95	60.43
270	58.94	62.52
280	60.94	64.59
290	63.11	66.80
300	65.36	69.08

* Metastable crystals.

TABLE III

MOLAL ENTROPIES AT 25°C.

0°C. = 273.16°K.

Azelaic Acid	
M.W. = 188.218	Cal./degree
$S_{(13.00)}$ (Debye, 6° freedom, $\theta = 122$)	0.370 ± 0.04
$S_{(13.00 - 298.16)}$, graphical	70.251 ± 0.077
$S_{(298.16)}$, solid	70.621 ± 0.11
Sebacic Acid	
M.W. = 202.244	
$S_{(13.93)}$ (Debye, 6° freedom, $\theta = 114$)	0.550 ± 0.066
$S_{(13.93 - 298.16)}$, graphical	77.410 ± 0.08
$S_{(298.16)}$, solid	77.960 ± 0.14

azelaic and sebacic acids. Summaries of these calculations are given in Table III.

Discussion

The heat capacity of azelaic acid shows no unusual features. On the other hand, sebacic acid shows a higher order transition between 130° and 153°K . An enlargement of the section of the heat capacity curve including this transition is shown in the inset of Figure 1.

This transition is unusual in several respects. Few materials with melting points as high as that of sebacic acid (134.5°C .) have transitions in such a low temperature range. Furthermore, the transition exhibits a marked hysteresis; the metastable high temperature form can be supercooled to about 115°K . The rate of transition is immeasurably slow above this temperature, but the rate increases rapidly with decreasing temperature. Thus, attempts to supercool the high temperature form below 110°K . were unsuccessful (i.e., the measurements which were made represented the heat capacity of unknown mixtures of both high and low temperature forms).

Some of the dihydrogen phosphates and arsenates⁴ have transitions in this temperature range. These transitions have been satisfactorily interpreted⁵ as a change from an ordered to a random arrangement of the hydrogen atoms in the hydrogen bonds between the $\text{H}_2\text{P}(\text{As})\text{O}_4^-$ groups. The authors believe that the transition found in sebacic acid can be given an analogous interpretation although there are not sufficient data to establish this proposition conclusively.

In many substances containing hydrogen bonds, there are a large number of possible configurations of the hydrogens in these bonds. If the number of accessible arrangements is \underline{W} , the entropy associated with this random-

ness is $k \ln W$. In ice and heavy ice this randomness persists even at extremely low temperatures because the allowed states are of nearly equal energy ("degeneracy" of the lowest state) and there is no observable tendency of the crystal to assume a unique configuration of zero entropy. However, the allowed states in some crystals do not all have nearly equal energies and a transition to an arrangement of lower energy and entropy may occur at an attainable temperature.

This interpretation has been confirmed for the dihydrogen phosphates and arsenates by the consideration of several fundamentally independent experiments. From the determination of the complete crystal structure of KH_2PO_4 ⁶, except for the location of the hydrogen atoms, it is evident that there is a unique configuration of lowest energy. In this arrangement of zero entropy, the crystal has a large permanent polarization which can be observed in the ferro-electric (Seignette-electric) properties of these crystals below the transition temperature (identical with the electric Curie point). Further, the entropy change which is observed to be associated with these transitions is approximately $k \ln W$, where W is the number of configurations predicted for the high temperature form.

A complete determination of the crystal structure of sebacic acid is not available for the discussion of its transition. However, from a consideration of the study of the unit cell and space group^{7,*} and of the structural chemistry of the carboxylic acids⁸, the structure shown in Figure 2 seems likely. In this structure the hydrogens in the

* X-ray diffraction photographs of the sebacic acid used in this investigation were made using a powder camera. Since all the observed lines were indexed within experimental error according to the unit cell and space group reported by Caspari, it is concluded that the crystalline forms of the two materials are probably identical.

APPROXIMATE ATOMIC ARRANGEMENT IN THE SEBACIC ACID CRYSTAL

(From the data of J. Caspari, J. Chem. Soc., 1928, 3235.)

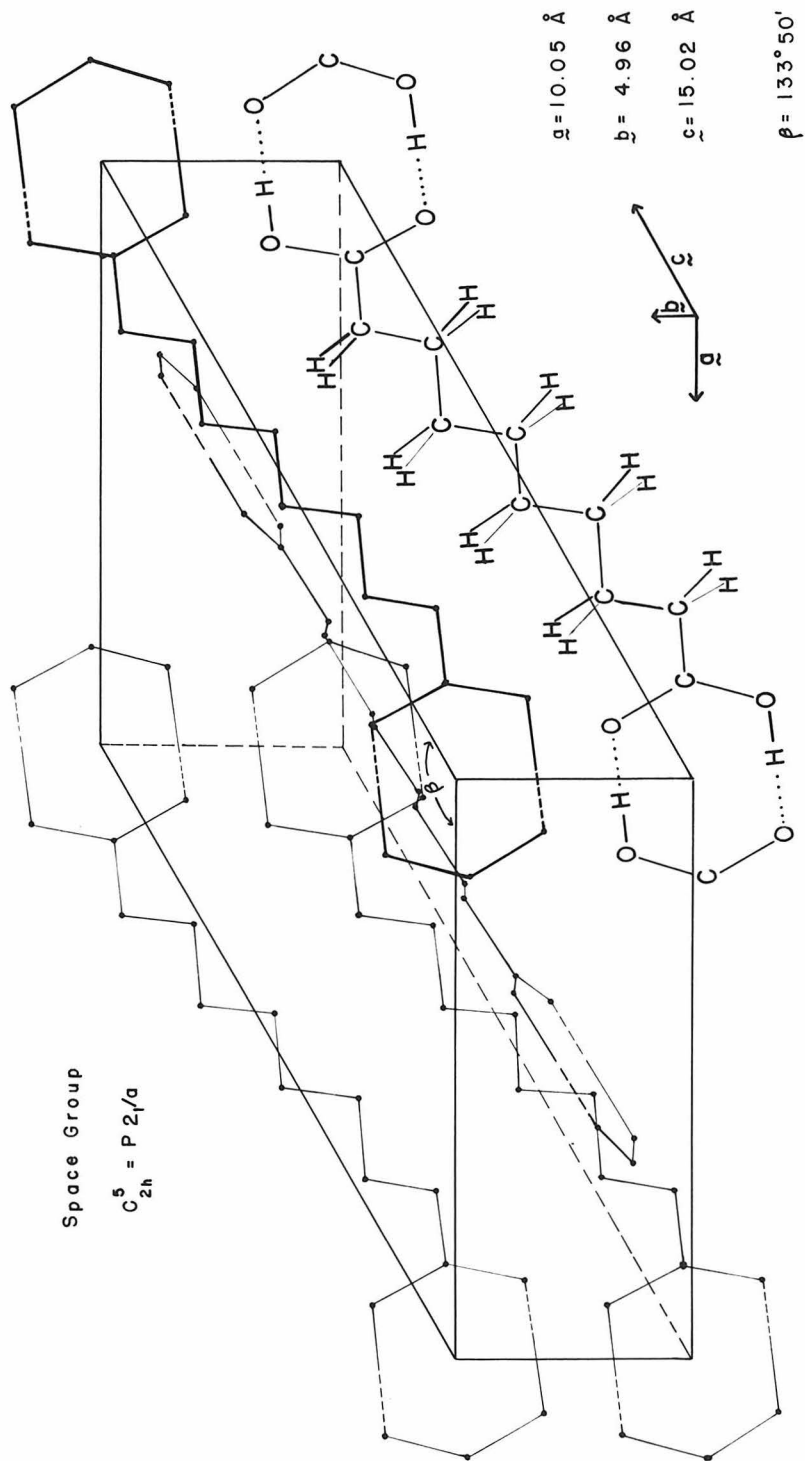
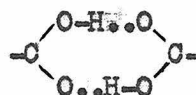


Figure 2

hydrogen bonds may be arranged in 2^N configurations in which there is one hydrogen nearest each carboxyl group; N is the number of molecules. Thus, the order-disorder entropy of this crystal is $Nk \ln 2 = 1.38$ e.u. From the experimental data it is estimated that the difference in entropy between the high and low temperature forms is less than 0.80 e.u.* This difference between experiment and theory may be attributed to (1) the failure of the crystal to attain complete randomness in the transition, (2) a state of limited order at low temperatures, or (3) both. In the following discussion it is concluded that the first suggestion is most likely.

It will be seen from Figure 2 that the centers of the



groups are arranged in two-dimensional nets separated by 15.02 \AA . There will be energy interactions between neighboring groups in a given net depending on the positions of the hydrogen atoms. (These interactions may be due to electrostatic or van der Waals forces.) In so far as these interactions within the net are concerned, each group has three pairs of neighbors. The strength of the interaction or coupling of each kind of neighbor to a given group depends on the orientation of the $-\text{COOH} \cdot \text{HOOC}-$

* It is not possible to extrapolate the heat capacity of the high temperature form to absolute zero with any certainty. One extrapolation was made by assuming that the heat capacity of the high temperature form could be represented by

$$C_p(\text{sebacic acid}) = (a - bT) C_p(\text{azelaic acid})$$

and by evaluating the constants a and b over the range 112° to 300° K. by least squares. The entropy difference calculated using this approximation is 0.82 e.u. of which 0.51 e.u. is obtained in the range $112-155^\circ$ K. where the high temperature form can be supercooled. The authors believe that this estimate is close to an upper limit. Further, it is believed that the lower limit of the entropy difference is approximately zero.

groups in the crystal and one or more of these couplings may be negligible. A given -COOH.HCOO- group will have lower energy if its hydrogens have the same configuration as that of the majority of the neighboring groups to which it is coupled.

The statistical mechanics of a two dimensional crystal with an order-disorder transition has been discussed by Onsager⁹ and is applicable to this crystal if the interactions of more distant neighbors than the nearest two pairs* within the net and the interactions between the nets are neglected. This treatment predicts a cusp in the heat capacity (third-order transition). In the case where the couplings of a group to its four nearest neighbors are equal, the entropy increment associated with the disordering of the hydrogens from the absolute zero to the singular temperature is 0.61 e.u.. Since the region of large absorption of heat involved in the order-disorder transition extends beyond the singular temperature, a further entropy increase would be attributed to the transition. The amount to be added is somewhat arbitrary as it is difficult to decide where the transition apparently ends. It is estimated by the authors that less than an additional 0.30 e.u.** would be attributed to the transition in most experiments. Thus, the total entropy change expected to be observed in the transition is less than 0.91 e.u. when the interactions of the four nearest neighbors is equal.

When the coupling to the two pairs of nearest neighbors are unequal, the cusp predicted in the heat capacity becomes sharper and the area below

* The extension of the theory to three pairs of neighbors is indicated but the results are not reported in Onsager's paper.

** This is the entropy between the singular temperature and the temperature where the heat capacity due to order-disorder falls to 0.25 cal./deg.

it decreases. In the limit when the effect of one pair of neighbors is negligible, there is a diffuse hump in the heat capacity extending over so many degrees that it would be difficult to recognize; and therefore at this limit no entropy change would be attributed to the transition. Thus, as the ratio of the interaction energy of one pair of neighbors to that of the other pair decreases, the apparent entropy of the transition would decrease from 0.9 e.u. to zero. A quantitative discussion for varying degrees of anisotropy of interaction will have to be the subject of further work, since Onsager did not report detailed computations in his paper.

The shape of the region of anomalous heat absorption observed in sebacic acid is not cusp-like, but a "smeared out" cusp would not be at variance with the observed shape. This "smearing out" could be due, in part, to the limitations of the experimental method, but it is more probably the result of crystal imperfections and possibly of the failure of the two dimensional model considering only the interactions of the four nearest neighbors. The entropy involved in the transition is qualitatively explained by the theory. A more quantitative comparison will have to await a fuller development of the theory of Onsager and the determination of the crystal structure of sebacic acid.

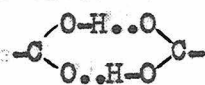
The failure of azelaic acid to exhibit a transition still remains to be explained. Only a small difference between the crystal structure of sebacic and azelaic acids would give rise to either of two effects. First, if one of the configurations of the $-COOH..HOOC-$ groups had a significantly greater energy than the other because of the steric hindrance of an oxygen of a neighboring group, there would be no randomness of the type discussed here. Second, if the interaction energy of one pair of neighboring groups were lessened, the cusp in the heat capacity would become so

small that it would be unobserved; or if the interaction energy of all four neighbors were weakened, the transition temperature would be lowered and not attained or the high temperature form would be "frozen in" as in ice. It is also possible that each carboxyl group is hydrogen bonded to two carboxyl groups as in β -oxalic acid, in which case no transition or randomness would be expected. It appears to the authors that no sound conjectures can be made until the complete crystal structures of these two compounds have been determined.

The authors now raise the old question whether the hydrogens in the hydrogen bonds in the carboxylic acids are arranged randomly or are arranged uniquely. If the interpretation presented here is correct, the answer is that for sebacic acid the low temperature configuration is practically unique. The entropy of randomness, $R \ln 2 = 1.38$, suggested by Pauling¹⁰ for carboxylic acids is therefore not included in the summaries of the entropy of azelaic and sebacic acids.

Summary

The heat capacities of azelaic and sebacic acids have been measured.

A higher order transition was observed in sebacic acid in the temperature range 120-153°K. It is suggested that this is an order-disorder transition of the two configurations of the hydrogens in the  groups in the crystals. This proposition is discussed with the aid of the theory of Onsager⁹.

The molal entropies of azelaic and sebacic acids were calculated for 298.16°K.; $S(\text{azelaic acid}) = 70.62 \text{ cal./deg.}$ and $S(\text{sebacic acid}) = 77.96 \text{ cal./deg.}$ These entropies do not include an amount $R \ln 2 = 1.38 \text{ cal./deg.}$ for the randomness of the arrangement of the carboxylic

hydrogens since arguments are presented that there is essentially no randomness at low temperatures.

Acknowledgment

One of the authors (G.G.) wishes to thank Prof. J. G. Kirkwood for bringing Onsager's paper to his attention. He also expresses his appreciation to Dr. J. Waser for criticism and discussion of this manuscript.

References

1. Parks, G. S., and Huffman, H. M., The Free Energy of Organic Compounds, A.C.S. Monograph Series No. 60, Chemical Catalog Co., New York (1932)
2. Succinic acid: Parks, G. S. and Huffman, H. M., J. Am. Chem. Soc., 52, 4381 (1930)
3. Ruehrwein, R. A. and Huffman, H. M., J. Am. Chem. Soc., 65, 1620 (1943)
4. Stevenson, C. C. and others, J. Am. Chem. Soc., 66, 1397, 1402, 1405, 1409 (1944)
5. Slater, J. C., J. Chem. Phys., 9, 166 (1941)
6. West, J., Z. Krist., 74, 306 (1930)
7. Caspari, K., J. Chem. Soc., 1928, 3235
8. Adipic acid: MacGillavry, C. H., Rec. trav. chim., 60, 605-17, (1941)
 β -Oxalic acid: Hendricks, S. B., Z. Krist., 91, 48 (1935)
Succinic acid: Verviel, H. J. and MacGillavry, C. H., Z. Krist., 102, 60, (1940)
9. Onsager, L., Phys. Rev., 65, 117, (1944)
10. Pauling, L., J. Am. Chem. Soc., 57, 2680 (1935)

PART II

THEORY OF THE THERMAL DIFFUSION OF ELECTROLYTES

IN A CLUSIUS COLUMN

THEORY OF THE THERMAL DIFFUSION OF ELECTROLYTES

IN A CLUSIUS COLUMN*

George Guthrie, Jr., J. Norton Wilson and Verner Schomaker

Abstract

A theory is presented which accounts approximately for the apparently anomalous difference between the thermal diffusion coefficients of the ions of an electrolyte in the presence and in the absence of other electrolytes; the theory is based on the electric field resulting from the variation in diffusion constant among the various ions present. An apparent deviation from the Debye exponential law is pointed out in some published data on the behavior of electrolytes in the Clusius column.

Introduction

An apparent anomaly in the thermal diffusion of electrolytes was reported by Gillespie and Breck¹ and by Hirota² in 1941. In experiments with the Clusius column³ these workers found that one** of a mixture of two electrolytes was transported into the upper reservoir, contrary to its behavior when it was the only solute; the other electrolyte of the mixture was transported as usual into the lower reservoir, but to a greater extent than when it was the only solute. Prior to this work no instances of the thermal diffusion of an electrolyte against the temperature gradient had been recorded in the literature.

* This section of the thesis is Contribution No. 1222 from the Gates and Crellin Laboratories of Chemistry and will be published in the Journal of Chemical Physics for February 1949.

** In these experiments the two electrolytes have a common ion.

A similar but less striking effect has long been known to occur in the ordinary diffusion of mixtures of electrolytes⁴; the more mobile of two mixed electrolytes diffuses more rapidly, the less mobile more slowly, than each diffuses alone. Vinograd and McBain⁵ accounted for the effect quantitatively in terms of an electrostatic field set up by the diffusion of ions of different mobilities. It occurred to one of us (G.G.) that the results of Gillespie and Breck and of Hirota could be similarly explained. We present herewith approximate treatments of the behavior of the mixed electrolytes in the pure Soret effect and in the Clusius column; the analysis accounts approximately for the anomalies referred to above.

The Soret Effect -- Thermal diffusion without convection.

Let the thermal gradient lie along the x axis. At the steady state the flux f_i of the i 'th ionic species across any plane in the solution normal to x will vanish, i.e.

$$f_i = -D_i dc_i/dx - D_i^! c_i dT/dx + \nu_i u_i c_i E = 0 \quad (1)$$

where D_i is the ordinary diffusion coefficient, $D_i^!$ is the thermal diffusion coefficient, c_i is the concentration in equivalents per unit volume, u_i is the equivalent mobility, ν_i is the sign of the ionic charge, and E is the local field postulated to arise from the difference in ionic mobilities.

Let us substitute $RTu_i = FD_i$, where F is the Faraday; multiply Equation (1) by ν_i/D_i , and sum over all ions. Applying the approximate neutrality condition $\sum \nu_i dc_i/dx = 0$ we obtain

$$(EF/RT) \sum c_i = (dT/dx) \sum \nu_i c_i D_i^!/D_i \quad (2)$$

and

$$\frac{d \ln c_i}{dx} = \left(-\frac{D_i}{D_i} + \frac{\nu_i \sum \nu_i c_i D_i / D_i}{\sum c_i} \right) \frac{dT}{dx} \quad (3)$$

For non-electrolytes the Soret coefficient σ is equal to the ratio $-D'/D$. We shall call this ratio for individual ions the intrinsic Soret coefficient σ_i^* . The observed Soret coefficient σ_i for an ion in an electrolyte is therefore

$$(d \ln c_i / dx)(dx/dT) = \sigma_i = \sigma_i^* - \nu_i \sum \nu_i c_i^* / \sum c_i \quad (4)$$

For a single electrolyte AX this becomes

$$\sigma_{AX} = \sigma_A = \sigma_X = \frac{1}{2}(\sigma_A^* + \sigma_X^*) \quad (5)$$

For a mixture of electrolytes AX and BX

$$\begin{aligned} \sigma_A &= \sigma_{AX} + [c_B / (c_A + c_B)] (\sigma_{AX} - \sigma_{BX}) \\ \sigma_B &= \sigma_{BX} + [c_A / (c_A + c_B)] (\sigma_{BX} - \sigma_{AX}) \end{aligned} \quad (6)$$

Equations (6) predict effects of the type observed by Gillespie and Breck and by Hirota. The electrolyte which has the higher Soret coefficient alone will have an enhanced Soret coefficient in the mixture; that with the lower Soret coefficient alone will have a diminished coefficient in the mixture and may even have the sign of its coefficient reversed if the difference between σ_{AX} and σ_{BX} is sufficiently great. Unfortunately no data are available for a direct test of these equations.

Thermal Diffusion with Convection

In the Clusius column a thermal gradient is maintained between two parallel vertical walls set close together; a convection current is thereby

superimposed on the thermal diffusion current and the solute diffusing to the cold wall is carried to the bottom of the column and concentrated there.

Let the vertical coordinate be y with origin at the bottom of the column of height h . Let the temperature gradient be parallel to the coordinate x with origin mid-way between the walls, separated by a distance $2a$.

A material balance for an element of volume of height dy and unit width extending normal to the y axis from $x = 0$ to $x = a$ leads at the steady state to

$$- D_i \partial c_i / \partial x - D_i^* c_i \partial T / \partial x + \nu_i D_i c_i FE x / RT - \int_0^a v_y(x) [\partial c_i(x) / \partial y] dx = 0 \quad (7)$$

where v_y is the vertical component of the convection current and all concentrations unless otherwise specified refer to the values at $x = 0$. Effects of diffusion arising from $D \partial c / \partial y$ have been neglected as small compared to $v_y \partial c / \partial y$.

Since $\partial c / \partial y$ is not likely to vary markedly with x , we may to a good approximation replace the integral in (7) with $a \bar{v}_y \partial c / \partial y$ where \bar{v}_y is the mean velocity of the convection current between $x = 0$ and a .

The field E may be evaluated as before in any one of several ways; the accuracy and convenience of the result depends on which of the terms is eliminated in the summation. We choose to eliminate $\sum \nu_i \partial c_i / \partial y$ and obtain

$$\frac{FE}{RT} = \frac{\sum \nu_i D_i \partial c_i / \partial x + (\partial T / \partial x) \sum \nu_i D_i^* c_i}{\sum D_i c_i} \quad (8)$$

whence

$$\bar{a}\bar{v}_y \partial c_i / \partial y = - \left(D_i \partial c_i / \partial x - \frac{v_i D_i c_i \sum v_i D_i \partial c_i / \partial x}{\sum D_i c_i} \right) - \frac{\partial T}{\partial x} \left(D_i^1 c_i - \frac{v_i D_i c_i \sum v_i D_i^1 c_i}{\sum D_i c_i} \right) \quad (9)$$

A consideration of the divergence of the flux in a volume element of cross-section $dydx$ at $x = 0$ indicates that $\partial c_i / \partial x$ at $x = 0$ is small. To a fair approximation we may set $(\partial c_i / \partial x)$ equal to $\varphi c_i \sigma_i dT/dx$ for all ions, where φ is a constant lying between zero and unity and σ_i is defined by Equation (4). This relation has been shown by de Groot⁶ to hold approximately in the thermal diffusion of non-electrolytes in the Clusius column. Substitution of this approximation in (9) by means of Equation (3) leads to

$$\frac{\partial c_i}{\partial y} = \frac{-(1 - \varphi)dT/dx}{\bar{a}\bar{v}_y} \left(D_i^1 c_i - \frac{v_i D_i c_i \sum v_i D_i^1 c_i}{\sum D_i c_i} \right) \quad (10)$$

Equation (10) can be integrated for the case of a single electrolyte, AX , if the dependence on y^* of the mobilities, thermal diffusion coefficients and average convection velocity can be neglected. Application of the conservation condition $\int_0^h \underline{c} dy = \underline{h}c_0$, where c_0 is the initial concentration of electrolyte, then leads to

$$R_{AX} = \ln (c_b/c_t)_{AX} = \left(\frac{c_b - c_t}{c_0} \right)_{AX} = K_{AX} h \left(\frac{D_A^1 u_X + D_X^1 u_A}{u_A + u_X} \right) \quad (11)$$

where R is called the enrichment. The quantities c_b and c_t are respectively

* The dependence on y either may be explicit or may be implicit through dependence on c .

the concentrations at the bottom and top of the column; K_{AX} is a constant whose magnitude depends on the dimensions of the apparatus and on the density, thermal expansion coefficient, and viscosity of the solution.

In the integration of Equation (10) for a mixture of two electrolytes, AX and BX , it is convenient to substitute $c_X = c_A + c_B$, and to substitute for the expressions in $u_i D_j^i$ in terms of the quantities $R_{ij}^i = R_{ij} K_m / K_{ij}$. Equation (10) becomes for this case

$$-\frac{\partial c_A}{\partial y} = \frac{c_A}{h} \left\{ \frac{(u_A + u_X) R_{AX}^i c_A + [(u_A + u_X)(u_B + u_X) R_{AX}^i - u_A (u_B + u_X) R_{BX}^i] c_B / u_X}{(u_A + u_X) c_A + (u_B + u_X) c_B} \right\} \quad (12)$$

A similar expression for $\partial c_B / \partial y$ is obtained by interchanging the subscripts A and B .

These expressions can be integrated approximately if the fraction in curly brackets is assumed to be constant, giving

$$R_A = \frac{[(u_A + u_X) R_{AX}^i] c_A + [(u_A + u_X)(u_B + u_X) R_{AX}^i - u_A (u_B + u_X) R_{BX}^i] c_B / u_X}{(u_A + u_X) c_A + (u_B + u_X) c_B} \quad (13)$$

and the corresponding expression for R_B . When the enrichments are great enough to invalidate this approximation, an exact integration may be made.

Variables may be separated in terms of the parameter $V = c_A / c_B$.

Integration of dv/dy and dc_B/dv yields

$$-\frac{y + y_0}{h} = \frac{u_X (u_A - u_B) \ln(1 + V)}{(u_A + u_X)(u_B + u_X)(R_{AX}^i - R_{BX}^i)} + u_X \ln V$$

and (14)

$$\ln kc_B = \frac{[u_A (u_B + u_X) R_{BX}^i - u_B (u_A + u_X) R_{AX}^i] \ln(1 + V) + u_X (u_B + u_X) R_{BX}^i \ln V}{(u_A + u_X)(u_B + u_X)(R_{AX}^i - R_{BX}^i)}$$

where y_0 and k are integration constants determined by the ratio and absolute magnitudes of the initial concentrations respectively. The limits of integration y_t and y_b are determined by the relation $y_t - y_b = h$.

In obtaining Equation (12) from Equation (11) it has been assumed that the quantities u and D' for each ion are constant. This assumption is justified even approximately only if the solutions of AX , BX , and of the mixture have the same ionic strength. Fortunately, this requirement is met in the experiments of Hirota. For dealing with more complicated situations such as are presented by the experiments of Gillespie and Breck a more complex equation corresponding to Equation (12) can be obtained in which the values u and D' corresponding to the different ionic strengths enter specifically. The variations in mobilities with ionic strength can be predicted fairly well, but no adequate theory appears to be available for the prediction of variations in D' .

Application to Experiment

The experimental enrichments obtained by the authors cited are compared in Table I with the values predicted by means of Equations (13,14) with substitution of the concentrations corresponding to the initial composition of the solutions, of mobilities corresponding to infinite dilution, and of a temperature midway between those of the hot and cold walls and of $\frac{R'_{AX}}{R_{AX}} = \frac{R'_{BX}}{R_{BX}}$. We have presented the results of the approximate integration, Equation (13), for all of the experiments. The more exact integration, Equation (14), was computed only for the experiments of Gillespie and Breck, in which the enrichments were large. In this computation $\frac{K_m}{K_{AX}}$ was assumed equal to $\frac{K_{AX}}{K_{AX}}$; this may be only a rough approximation.

In the data presented by Gillespie and Breck, $\ln c_b/c_t$ does not equal $(c_b - c_t)/c_0$ for single electrolytes; that is, the variation of concentration with height is not purely exponential as predicted by Equation (11). This complication may contribute to the disagreement between these data and the approximate theory presented here. It is not possible to choose at this time between the substitution of $\ln c_b/c_t$ and $(c_b - c_t)/c_0$ for the enrichment R. For the experiments of Gillespie and Breck we have made calculations using both values. It will be seen that the agreement is much better with Hirota's data, as is to be expected from the arguments given above.

It also may be mentioned that the results obtained by Gillespie and Breck and by Hirota can be accounted for by assuming that the enrichments of the various ions are proportional to their corrected Soret coefficients as given by Equation (6). The enrichments computed on the basis of this assumption are given in Column 3 of Table I; we are unable to present a detailed explanation for their excellent agreement with the experimental results, although the result perhaps may be a natural consequence of the small separations obtained together with good equilibration along the temperature gradient.

Acknowledgment

The authors wish to express their appreciation to Prof. J. G. Kirkwood and to Prof. Leverett Davis, Jr. for helpful discussions and advice.

TABLE I

Solution	Ion	Enrichment					Observer
		$\frac{c_b}{c_t}$			$\frac{(c_b - c_t)}{c_o}$		
		Expt.	Theory	Soret*	Expt.	Theory	
1 N HCl	H ⁺ , Cl ⁻	1.22					Hirota**
1 N NaCl	Na ⁺ , Cl ⁻	1.047					
1 N NH ₄ Cl	NH ₄ ⁺ , Cl ⁻	1.010					
0.5 N HCl	H ⁺	1.34	1.43 ^{a,c}	1.32			Gillespie and Breck
0.5 N NaCl	Na ⁺	0.97	0.95 ^{a,c}	0.97			
0.5 N HCl	H ⁺	1.42	1.51 ^{a,c}	1.34			
0.5 N NH ₄ Cl	NH ₄ ⁺	0.89	0.88 ^{a,c}	0.89			
1 N HCl	H ⁺ , Cl ⁻	9.4			1.60		
1 N FeCl ₂	Fe ⁺⁺ , Cl ⁻	1.30			0.23		
1 N HCl	H ⁺	39.	72. ^{a,c}	25.	1.90	4.30 ^{a,c}	
1 N FeCl ₂			296. ^{a,d}			2.74 ^{a,d}	
			20.4 ^{b,c}			3.01 ^{b,c}	
			36.4 ^{b,d}			2.74 ^{b,d}	
			Fe ⁺⁺			0.92	0.40 ^{a,c}
		0.55 ^{a,d}			-0.52 ^{a,d}		
			0.55 ^{b,c}			-0.59 ^{b,c}	
			0.62 ^{b,d}			-0.44 ^{b,d}	

* Enrichment assumed proportional to effective Soret coefficient

** All measurements by Hirota listed above were made after his column had been running for two hours. The two-hour values did not differ greatly from the equilibrium values in these cases for which both were obtained; e.g. for 1 N NaCl, 1 N NH₄Cl, and 1 N HCl the equilibrium values were respectively 1.048, 1.010, and 1.25 as compared to values of 1.047, 1.010, and 1.22 at two hours.

(a) Using $\underline{R} = \ln(\frac{c_b}{c_t})$ (c) Approximate integration, Equation (13)

(b) Using $\underline{R} = \frac{(c_b - c_t)}{c_o}$ (d) Exact integration, Equation (14)

Appendix

The Apparent Distribution of Solute in Gillespie and Breck's
Column

Evidence will now be presented which suggests that the concentration of solute at the steady state in Gillespie and Breck's apparatus approximates more closely a linear dependence on the vertical coordinate than the exponential dependence which was predicted by Debye⁷ and which also follows from the treatment presented here.

Applying the conservation condition to a column without reservoirs as used by Gillespie and Breck we have for the exponential distribution,

$$c = u(x) \exp(\alpha y) \quad ,$$

the consequence $(c_b - c_t)/c_o = \ln(c_b/c_t)$ (15)

where c_o is the initial concentration.

For a linear distribution of concentration up the column,

$$c = u(x)(1 + \beta y) \tag{16}$$

$$(c_b - c_t)/c_o = 2(c_b/c_t - 1)/(c_b/c_t + 1)$$

The experimental values of $(c_b - c_t)/c_o$ and c_b/c_t , both of which were reported by Gillespie and Breck, are presented in Table II together with the values of c_b/c_o calculated by means of Equations (15) and (16) from the experimental values of $(c_b - c_t)/c_o$. The results shown in Table II indicate that the distribution of solute up the column is certainly not exponential and may be roughly linear.

We are unable to account for the apparently linear distribution; a

TABLE II

Solution and Ions	$\frac{c_b - c_t}{c_o}$	$\frac{c_b}{c_t}$		
	Expt..	Expt..	Calculated Linear Exponential	
0.5 M FeCl ₂	0.22	1.29	1.25	1.25
0.5 M BaCl ₂ } Ba ⁺⁺	0.44	1.64	1.57	1.55
+ 1 M HCl } H ⁺	1.06	3.9	3.26	2.88
1 M HCl	1.60	9.4	9.0	4.95
1 M HCl } H ⁺	1.90	39	39	6.69
+ 0.5 M FeCl ₂				

function linear in y is not a valid solution for the differential equation which applies to a column in which only laminar convection occurs. Possibly in Gillespie and Breck's apparatus $\frac{v}{y}$ varied appreciably with y . It is quite possible, also, that the apparent agreement with a linear distribution is purely coincidental; indeed, some of their data appear to require a dependence of c on y whose curvature is of the opposite sign from that of the exponential.

References

1. Gillespie, L. J. and Breck, S., J. Chem. Phys., 9, 370 (1941)
2. Hirota, K., Bull. Chem. Soc. Japan, 16, 232 (1941)
3. Clusius, K. and Dickel, G., Naturwiss., 26, 546 (1938)
4. Graham, T., Phil. Trans. Roy. Soc. (London), 805 (1850)
McBain, J. W., and Dawson, C. R., J. Am. Chem. Soc., 56, 52 (1934)
5. Vinograd, J. R., and McBain, J. W., J. Am. Chem. Soc., 63, 2008 (1941)
6. de Groot, S. R., L'Effet Soret, N.V. Noord-Hollandsche Uitgevers Maatschappij, Amsterdam, 1945, p. 107.
7. Debye, P., Ann. Phys., 36, 284 (1939)

PART III

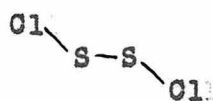
A STUDY OF THE STRUCTURE OF SULFUR MONOCHLORIDE
BY ELECTRON DIFFRACTION

A STUDY OF THE STRUCTURE OF

SULFUR MONOCHLORIDE

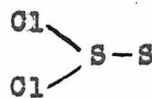
BY ELECTRON DIFFRACTION

The structure of sulfur monochloride, S_2Cl_2 , has been a subject of controversy for many years. Chemists have assigned either or both of two structures to this compound. In structure I, which will be called the chain structure, the two chlorine atoms are bonded to different sulfur atoms, while structure II, which will be called the pyramid structure, is analogous to thionyl chloride in that both chlorine atoms are bonded to a single sulfur atom.



I

(chain)



II

(pyramid)

Interpretations of the structure of this compound by means of chemical reactions appear to be inconclusive since for either structure reactions can be cited which seem to favor it. A survey of the studies of this structure by many physical chemical methods, including Raman spectra¹, dipole moment², magnetic susceptibility³, ultra-violet absorption spectra⁴, exchange with radioactive sulfur⁵, and electron diffraction of the gas⁶, shows that the conclusions reached do not favor preponderantly one structure or the other. Although a critical examination of these studies is beyond the scope of this research, it should be pointed out that some of the investigators have shown merely that their observations

are consistent with the only structure considered.

Since only the interatomic distances can be determined by electron diffraction of gases, the location of the bonds must be found indirectly. If the interatomic distances determine a unique geometric configuration, there is usually only one reasonable assignment of bonds. However, the geometric configuration of molecules having more than three atoms is not always uniquely described by the interatomic distances alone. In the case of sulfur monochloride, the chain structure can be distinguished unambiguously only if the Cl \cdots Cl distance is greater than $2(S-Cl)\sin \angle Cl-S-S$ (approximately 4.0 Å). Hence, a direct distinction between the chain (I) and pyramid (II) structures rests on the determination of the Cl \cdots Cl distance.

Two previous studies by electron diffraction of sulfur monochloride⁶ have been reported. Ackermann and Mayer were unable to determine the Cl \cdots Cl distance but assumed the chain (I) structure and reported the following parameters: average $(S-Cl = 1.98 \text{ Å}, S-S = 2.04 \text{ Å}) = 2.00 \text{ Å}$ and $S \cdots Cl = 3.19 \text{ Å}$. In a more recent investigation based on a greater range of observation, Palmer reported a peak in his radial distribution function corresponding to a Cl \cdots Cl distance of 3.97 Å and concluded that the molecule has the chain (I) structure. In addition to the Cl \cdots Cl distance Palmer has reported the following parameters: $S-Cl = 1.99 \text{ Å}$ (assumed from $SOCl_2$), $S-S = 2.05 \text{ Å}$, $(\overline{S-Cl}, S-S = 2.01 \text{ Å})$, $S \cdots Cl = 3.18 \text{ Å}$ ($\angle Cl-S-S = 105^\circ$), and the angle between the two Cl-S-S planes = 97° . However, he was unable to confirm the reality of the Cl \cdots Cl distance by the correlation procedure. He was unable to exclude a trans configuration ($Cl \cdots Cl = 4.97 \text{ Å}$) and concluded that

a freely rotating model was possible. It has been found⁷ subsequently that a radial distribution function of the type used by Palmer would be expected to show a spurious peak at approximately the distance reported by Palmer. Bauer⁸ stated recently that he was almost unable to distinguish between chain and pyramid structures by electron diffraction alone. This conclusion has been confirmed in the present investigation over the range of Palmer's observations ($q = 12$ to $q = 63$), where models which were equally acceptable could be found based on either structure. Since Palmer, by considering only the chain structure in his correlation treatment, did not show that the pyramid structure was unacceptable, the reinvestigation of this molecule was undertaken.

Material. The sulfur monochloride was prepared by the direct reaction of chlorine on sulfur. The crude product was distilled twice in vacuo in an all glass system from liquid enriched in sulfur.

Apparatus and Method. Photographs were taken using the electron diffraction camera described by Brockway⁹. An all-glass heated nozzle built by Claesson¹⁰ was used and pictures were taken with nozzle temperatures of 85°C. and 250°C. The camera (jet to film) distance was 10.95 cm. The electron wavelength as determined from ZnO photographs¹¹ was 0.0608 Å.

About thirty usable pictures were obtained, and on some it is possible to observe rings to the edge of the camera. The high and low temperature pictures have no observable differences and all pictures are indistinguishable in appearance from those taken by Palmer^{6b}. Ten rings were observed and a total of thirty-three features were measured. The measured positions of maxima and minima are listed in Table I. Visual curves were drawn and radial distribution functions were calculated¹².

TABLE I

Observed and Calculated Maxima and Minima

Max.	Min.	Observed	Model T	q_1/q_0	Weight
	1	4.48	4.80	1.0715	1
1		6.53	6.95	1.0644	3
	2	9.00	8.85	0.9833	2
A		11.38	11.55	1.0150	3
2		13.41	13.30	0.9918	7
	3	17.30	17.40	1.0063	9
3		20.36	20.78	1.0206	5
	4	23.22	23.40	1.0077	5
4		25.81	25.60	0.9919	5
	5	28.91	28.10	0.9720	5
5		32.59	32.40	0.9942	10
	6	36.29	36.45	1.0044	10
6		39.83	40.28	1.0088	7
	7	41.70	41.60	0.9976	7
7		43.95	43.55	0.9909	7
	8	47.70	47.40	0.9937	10
8		51.48	51.68	1.0039	10
	9	55.00	55.45	1.0082	5
9		57.92	57.98	1.0010	5
	10	60.15	60.15	1.0000	5
10		62.91	62.65	0.9959	5
	11	66.44	66.60	1.0016	10
11		70.40	70.60	1.0020	10
	12	72.94	73.78	1.0115	5
12		75.10	76.30	1.0160	4
	13	77.63	78.20	1.0073	4
13		81.58	81.90	1.0039	7
	14	86.22	87.78	0.9948	6
14		88.03	89.65	1.0184	3
	15	90.69	91.80	1.0105	3
15		92.60	93.30	1.0076	2
	16	95.66	97.28	1.0169	3

average $q_1/q_0 = 1.0028$

average deviation = 0.0087

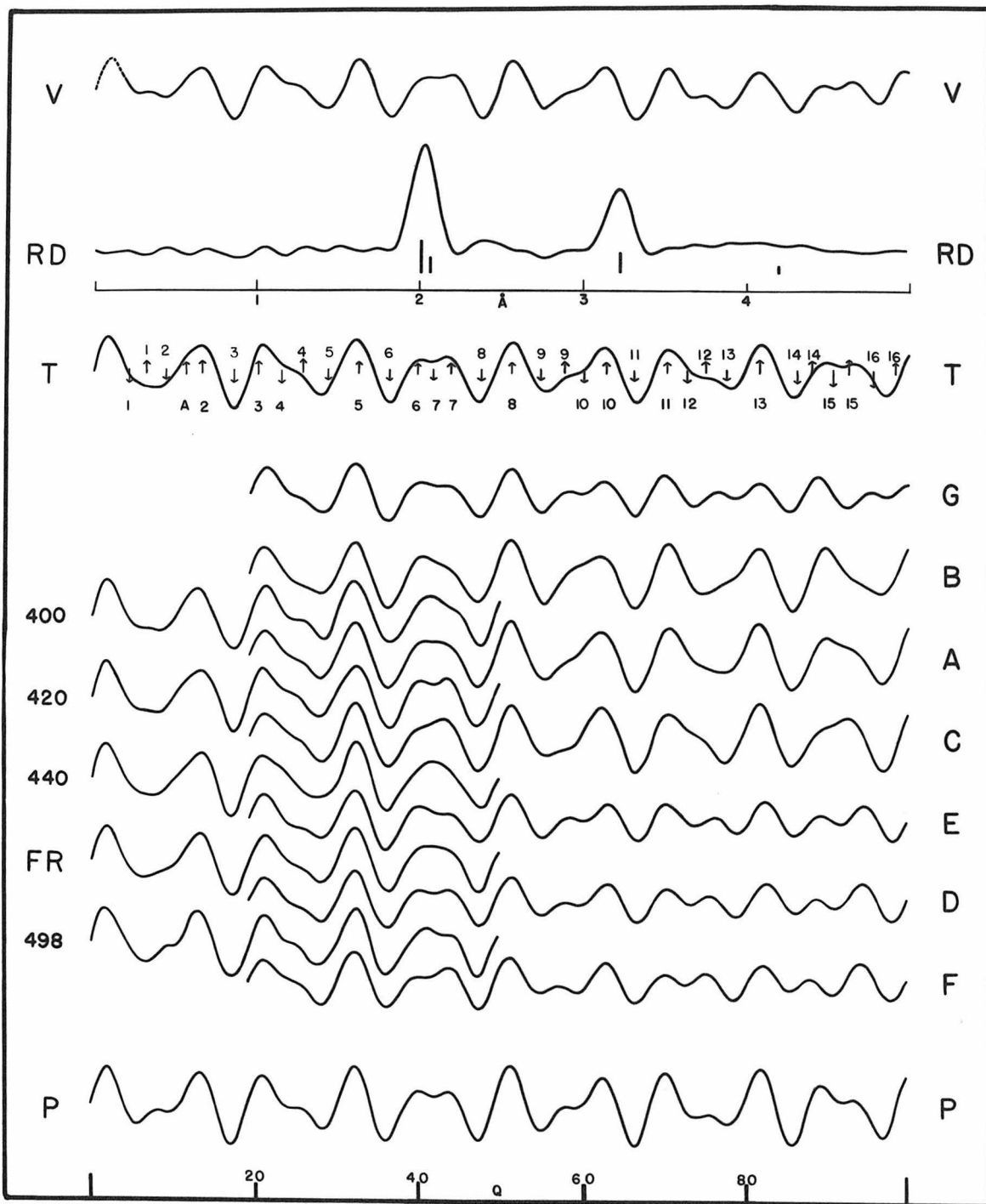
Interpretation of the radial distribution function led to satisfactory models. The best model and limits of error were found by the correlation method using theoretical curves calculated by means of the reduced intensity function

$$qI(q) = \sum_i \sum_{j \neq i} (Z_i Z_j / r_{ij}) \sin r_{ij} q, \quad (1)$$

$$q = 10\pi/\lambda = 40/\lambda \sin \theta/2.$$

The Visual Curve. Curve W in Figure 1 represents the interpretation of the visual appearance of the photographs. Theoretical curves were used as a guide in estimating the relative height of the central maximum and depth of the first minimum since a large error was made in the original estimate of these features. However, it is believed that the drawing of the visual curve has not been unduly influenced by calculated curves; all that is essential in the visual curve corresponds faithfully to original judgments and measurements.

Results. It is expected that the S-Cl, S-S, and S^o-Cl distances should not be greatly different in the two (chain and pyramid) structures and that a decision between the structures would be most clearly indicated by the determination of the Cl^o-Cl distance. The radial distribution function (RD in Figure 1) shows two strong nearly symmetrical peaks at 2.03 Å. and 3.22 Å., but there is no feature which can be identified definitely as the Cl^o-Cl distance. There is a low, very broad peak which might be interpreted as a long (about 4. Å.) distance with a large temperature factor. However, this peak may be spurious since its height is of the order of magnitude of the uncertainty in the base line. Since the relative areas of isolated peaks are sometimes in error by as much as a



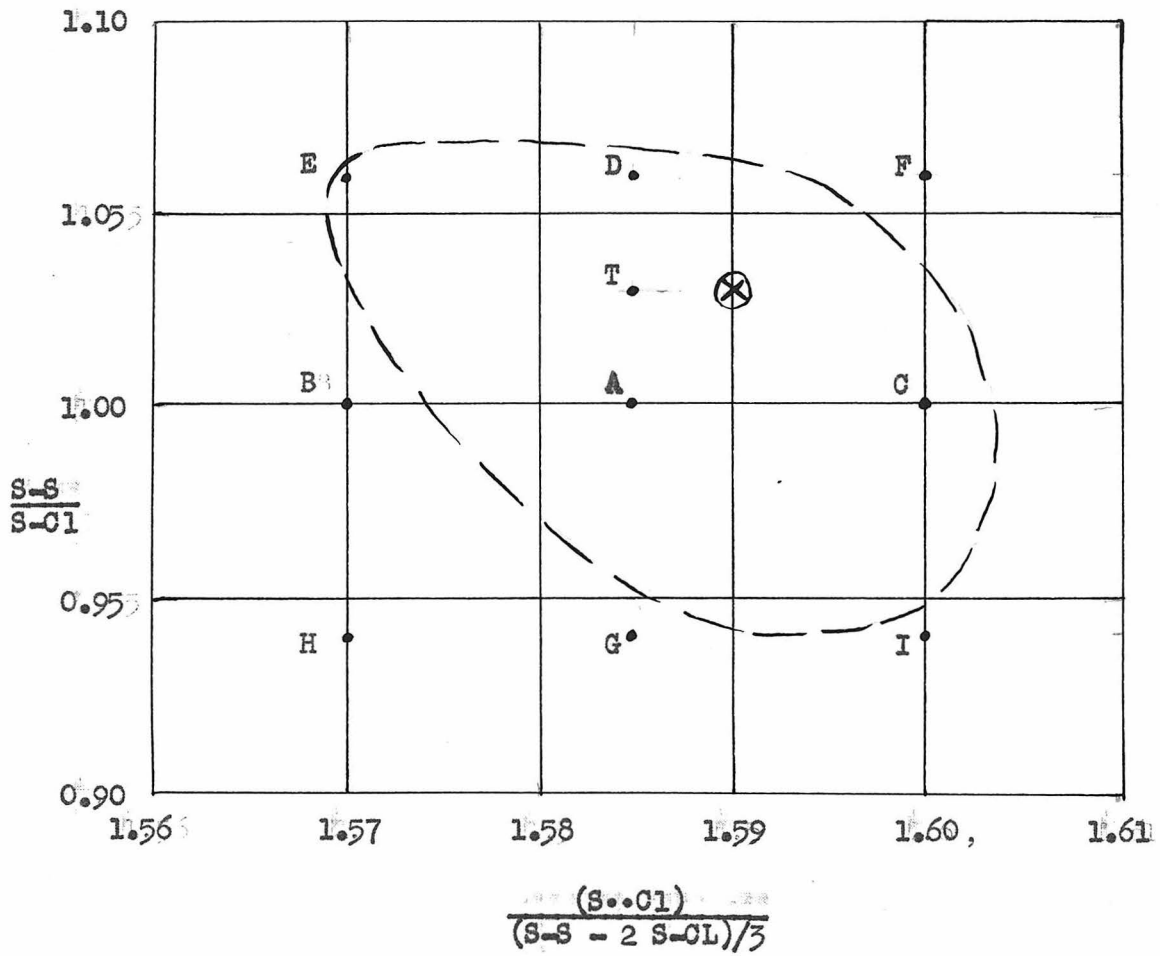
Electron Diffraction Curves for Sulfur Monochloride

Figure 1.

TABLE II

Parameters of Models Calculated

Model	S-O1	S-S	S..O1	Cl..O1
A	2.03 Å	2.03 Å	3.220 Å	—
B	2.04	2.04	3.205	—
C	2.022	2.022	3.235	—
D	1.99	2.11	3.220	—
E	2.00	2.12	3.205	—
F	1.98	2.10	3.235	—
G	2.07	1.95	3.220	—
H	2.08	1.96	3.205	—
I	2.06	1.94	3.235	—
FR	2.03	2.03	3.220	free rotation
P	2.03	2.03	3.220	3.22
400	2.03	2.03	3.220	4.00
420	2.03	2.03	3.220	4.20
440	2.03	2.03	3.220	4.40
498	2.03	2.03	3.220	4.98
T	2.005	2.065	3.222	4.20 with temperature factor $\exp(-as^2)$, $a = 0.0034$



Field of Parameters for Models A to I and Model T

Figure 22

factor of two, an alternative interpretation is that the $\text{Cl}^{\circ}\text{Cl}$ is included within the 3.22 \AA . peak. It was concluded on the basis of the radial distribution function that the $\text{Cl}^{\circ}\text{Cl}$ distance may be approximately either 4.15 \AA . or 3.22 \AA ., but a definite decision could not be made.

Theoretical curves were calculated for three sets of models, with the distances listed in Table II. In all sets the S-Cl, S-S, and S $^{\circ}$ -Cl distances in the central model were 2.03 \AA ., 2.03 \AA ., and 3.22 \AA . respectively. No $\text{Cl}^{\circ}\text{Cl}$ term was included in one set, represented by models A to G in Figure 1. The parameters for the members of this set are plotted on the map in Figure 2. These curves are practically indistinguishable from models in which the two chlorine atoms are rotating freely around the S-S bond, as represented by FR. Alternatively, at large q they represent structures in which the $\text{Cl}^{\circ}\text{Cl}$ distance has a large temperature factor. A second set was calculated in which the $\text{Cl}^{\circ}\text{Cl}$ distance was varied around 3.22 \AA .; model P is typical of this group and represents either a pyramid structure or a chain structure with nearly *cis* configuration. These two sets of models are practically indistinguishable in visual appearance. Both sets are qualitatively in good agreement with the visual curve beyond $q \sim 15$, and the average deviations of the ratio of the calculated to the observed position of features in this range are of the order of one percent for models in both sets although the deviations in the second set are slightly smaller. However, in the region $q \sim 15$ both sets are unsatisfactory in appearance and in the positions of the measured features. In the third set, models 400, 420, and 440, the $\text{Cl}^{\circ}\text{Cl}$ distance was varied around 4.20 \AA . corresponding to chain structures. This set of models gives much better agreement in the region of the first minimum than either

of the other two sets and is quite satisfactory out to about $q_0 = 35$. One other model has been calculated; 498 is a chain structure with the trans configuration. It is unsatisfactory.

It is concluded that the $C1 \cdot \cdot C1$ distance is about 4.2 \AA and has a large temperature factor. Comparison of models 400, 420, and 440 (illustrated in Figure 1 out to $q_0 = 50$) and models A to I (H and I not shown) with the visual curve V shows that the long term makes no significant contribution beyond $q_0 \sim 50$. Hence, the parameters $S-C1$, $S-S$, and $S \cdot \cdot C1$ can be determined nearly independently of the $C1 \cdot \cdot C1$ distance by correlation of the theoretical curves beyond $q_0 \sim 50$ with the visual curve and the measured maxima and minima. The visual appearance of model A is the most satisfactory. Models C and D are slightly better than E and I which are just acceptable. Models B, F, G, and H cannot be accepted. The average deviations of the quantitative comparisons rule out models B and H while models E, G, and I are barely acceptable. The best values and the limits of error of the shape parameters are (1) for the ratio of the average length of the $S-C1$ and $S-S$ bonds to the $S \cdot \cdot C1$ distance, $1.590 \pm 0.015 - 0.020$ and (2) for the ratio of the length of the $S-S$ distance to the $S-C1$ bond length, $1.035 \pm 0.04 - 0.09$. The limits of error are interdependent and are plotted on the parameter map in Figure 2. The distances* corresponding to the range of acceptable model shapes as defined by these ratios are found to be $(S-S + 2S-C1)/3 = 2.028 \pm 0.03 \text{ kX}$, $S-C1 = 2.01 \pm 0.09 - 0.06 \text{ kX}$, $S-S = 2.07 \pm 0.08 - 0.15 \text{ kX}$, and $S \cdot \cdot C1 = 3.224 \pm 0.03 \text{ kX}$. The $S-S-C1$ angle is $104.5 \pm 3 - 2^\circ$.

* The assigned limits of error include the uncertainty in the determination of the size.

The theoretical scattering function out to $q = 38$ is practically insensitive to changes in the S-Cl, S-S, and S $\cdot\cdot$ -Cl distances in the range of acceptable models; consequently, the long distance can be determined in this range by varying the Cl $\cdot\cdot$ -Cl term alone around a central model (such as A). Since there are relatively few observations in this range, this distance cannot be determined with the usual precision. Model 420 is the best of those calculated, and 400 is fairly acceptable, but 440 seems to be just beyond acceptability both in appearance and in the location of features. It is concluded that the best value of the Cl $\cdot\cdot$ -Cl distance is 4.15 Å with a limit of error of about 0.2 Å. The angle between the S-S-Cl planes is $92 \pm 12^\circ$.

It is estimated that the temperature factor, $\exp(-as^2)$, reduces the contribution of the long term by 50% at $q = 45$; i.e., $a = 0.0034$. Model T, whose parameters are near to the best values, has been calculated using this temperature factor and is shown in Figure 1. The calculated positions of maxima and minima for this model are given in Table I along with the ratios $q_{\text{calc.}}/q_{\text{obs.}}$ and their average deviations.

Discussion. The distances found in this molecule will fit only a chain structure. This result rests on the finding of a relatively long (> 4.0 Å) Cl $\cdot\cdot$ -Cl distance. The definite conclusion that the molecule has a long Cl $\cdot\cdot$ -Cl distance depends largely on measurements and interpretations inside the first major ring. Although such observations are less reliable in this region than between $q = 20$ to $q = 60$, the evidence is more than sufficient to make a definite decision. The first major minimum is shallow, quite flat, and broad. It is certain that $1\uparrow$ is unusually weak and does not lie on the outside, although it is possible that it lies at the bottom.

The first ring is broader than $3\uparrow$ or $5\uparrow$, rounded, and of moderate height with a very weak hump, $A\uparrow$, on the inside. Both $1\uparrow$ and $A\uparrow$ are drawn with slight exaggeration in the visual curve. Only models 400, 420, and 440 show all these features. In both models P and FR, $1\uparrow$ lies on the outside of the minimum, $A\uparrow$ does not appear, and $2\uparrow$ is nearly as sharp as $3\uparrow$ and $5\uparrow$. In addition, $1\uparrow$ in model P is much too strong. Quantitative comparisons lead to the same conclusions; the calculated q values of $1\downarrow$, $1\uparrow$, and $2\downarrow$ for both P and FR are all too large, and the deviations are larger and in a different direction than usually experienced in this region. Further, the presence of a long distance significantly improves the appearance and position of $4\downarrow$ and $4\uparrow$. Model 498 deserves some attention, since Palmer was unable to distinguish a trans model such as this from a staggered model similar to 400. It appears that a model could be found which would be acceptable in the range of Palmer's observations ($q = 12$ to $q = 63$). However, this model is excluded by both the qualitative appearance of and the quantitative comparisons in the first major minimum.

Only two comparisons between the best model found in the present research and the model favored by Palmer have any meaning. One difference appears serious; the size of the molecule found here is about one and one-half percent larger than that reported by Palmer. No explanation of this discrepancy is offered at this time. The other significant comparison, that between the $S\cdot Cl / S=Cl, S-S$ ratios (Palmer, 1.58; here, 1.59) is well within the limits of error. Since the range of observation in the present study is nearly twice as large, the latter value is probably more accurate.

It is evident now that the $Cl\cdot Cl$ distance reported by Palmer was

not founded on his experiment. It is indeed fortuitous that his value is within the present limits of error.

The best model reported in this study is not necessarily the most probable since the S-S/S-Cl ratio may be varied over rather wide limits. Any estimate of this ratio based on S-S and S-Cl distances found in other molecules must wait until the uncertainty in the size parameter has been cleared up.

Smyth et al.² have proposed that sulfur monochloride is a mixture of the chain and pyramid structures. It appears in the present research that the staggered chain is at least the predominant structure if not the only one. In order to be compatible with the diffraction data the fraction of molecules having this configuration must be three-quarters or greater.

Summary. The structure of sulfur monochloride has been redetermined by electron diffraction.

Sulfur monochloride has an extended or chain structure, Cl-S-S-Cl, in which the chlorine atoms are staggered. The following distances and parameters were found: $(S-S + 2S-Cl)/3 = 2.028 \pm 0.03$ kX, S-Cl = $2.01 \pm 0.09 - 0.06$ kX, S-S = $2.07 \pm 0.08 - 0.15$ kX, S•Cl = 3.224 ± 0.03 kX, Cl•Cl = 4.15 ± 0.2 kX, and $\angle S-S-Cl = 104.5 \pm 3 - 2^\circ$. The angle between the S-S-Cl planes is $92 \pm 12^\circ$ as measured from the cis configuration.

The results have been compared with earlier determinations⁶. A discrepancy in the size of the molecule has been noted.

References

1. Matossi, F. and Aberhold, H., Z. Physik., 68, 683 (1931)
Venkateswaren, S., Indian J. Physics, 6, 275 (1931)
Meyer, J., Z. anorg. u. gem. Chem., 203, 146 (1931)
Morino, Y. and Mizushima, S., Sci. Papers Inst. Phys. Chem. Research, Tokyo, 82, 220 (1937)
Garding, H. and Westrick, R., Rec. trav. chim., 60, 701 (1941)
2. Morino, Y. and Mizushima, S., loc. cit.
Smyth, G. P., et al., J. Am. Chem. Soc., 62, 1219 (1940)
3. Clow, A., et al., Trans. Faraday Soc., 36, 1018 (1940)
Dharmetti, S. S., Proc. Indian Acad. Sci., 13A, 359 (1941)
4. Lorenz, L. and Samuel, R., Z. physik. Chem., B14, 219 (1931)
Asundi, R. K. and Samuel, R., Proc. Phys. Soc., 48, 28 (1936)
5. Cooley, R. A. and Yost, D. M., J. Am. Chem. Soc., 62, 2474 (1940)
6. Ackermann, G. and Mayer, J. E., J. Chem. Phys., 4, 377 (1936)
Palmer, K. J., J. Am. Chem. Soc., 60, 2360 (1940)
7. Stevenson, D. P. and Schomaker, V., J. Am. Chem. Soc., 61, 3173 (1939)
8. Bauer, S. H., J. Am. Chem. Soc., 69, 3194 (1947)
9. Brockway, L. O., Rev. Mod. Phys., 8, 231, (1936)
10. Claesson, S., Donohue, J. and Schomaker, V., J. Chem. Phys., 16, 207 (1948)
11. Lu, C. S. and Malmberg, E. W., Rev. Sci. Instruments, 14, 271 (1943)
12. Shaffer, P. A., Jr., Schomaker, V., and Pauling, L., J. Chem. Phys., 14, 659 (1946)

PART IV

A STUDY OF FACTORS IN THE DESIGN
AND USE OF AN ELECTRON DIFFRACTION CAMERA

ABSTRACT

The theoretical expression for the angular distribution of electrons scattered by gases cannot be recorded exactly by a camera of finite dimensions. Alterations in the function arise from two causes, first, uncertainties are introduced into the scattering angle, and second, the uncertainty in the measurement of the number of electrons is less than the function only in a finite range. The alterations produced by these effects place conflicting demands upon the designer of an electron diffraction camera.

In this study a theory of the effect of the uncertainties on the determination of interatomic distances in gaseous molecules is developed by means of Fourier transforms. An expression is obtained which it is hoped will enable the designer to make the best compromise among the uncertainties.

The magnitude of the angular uncertainties due to the camera dimensions, lens parameters, lens aberrations, stability of the power supply, and cathode temperature are given.

Multiple scattering is described in the language of Fourier transforms and an approximate interpretation is given.

The requirements for an electrical recording system in a partially idealized camera are discussed.

TABLE OF CONTENTS

Abstract	51
Introduction	54
Performance	59
Indeterminacy of the scattering angle	61
Class I spreading functions	61
Class II spreading functions	62
The form of the spreading function	63
Modification of the intensity	65
Complete expression for the transform of the approximate observed scattering function	68
Transforms of modified scattering functions	70
Components of an electron diffraction camera	72
The monokinetic electron source	72
The collimator	74
The diffraction zone	75
The recording device	75
Geometric theory of diffraction	77
First-order geometric theory of diffraction	77
Second-order geometric theory of diffraction	79
Electron lenses and their application to electron diffraction	83
Lens aberrations	83
Geometric aberrations	83
Chromatic aberrations	87

Space charge effects	88
Collimating lens	88
Projector lens	90
Multiple scattering	97
Estimation of scattering probabilities	97
Fourier transforms of m-tuple scattering functions in two dimensions	98
Relation between the one and two dimensional Fourier transforms	99
One dimensional Fourier transform of the multiple scatter- ing functions	100
Appendix	107
References	108

A STUDY OF FACTORS IN THE DESIGN
AND USE OF AN ELECTRON DIFFRACTION CAMERA

INTRODUCTION

In the design of an instrument a number of compromises must be made among conflicting theoretical and practical considerations. Thus, it is necessary to obtain information, both theoretical and empirical, about the operation of all the important elements of the apparatus. When all this material is collected along with practical information, the performance of the instrument is analyzed with respect to the factors involved in the design and the required compromises reached. The procedure of design carried to this point defines the scope of theoretical instrument design. The results of theoretical design must be interpreted with some caution, although if all the elements have been treated adequately, the analysis will describe the actual performance. Often, however, a theoretical design describes a partially idealized instrument and indicates the limits of realizable performance. The discussion of the design of an electron diffraction camera presented here is limited to theoretical design. The results obtained in this analysis are practical in part and ideal in part.

The theory of the diffraction of electrons has been worked out in detail several times. Since this material has been collected and reviewed elsewhere¹, only the final results need be given here. The complete expression for the diffraction of fast electrons by gas molecules is

$$\Phi(\vartheta) d\omega = N j_i Q(\vartheta) d\omega \quad (1a)$$

where $\Phi(\theta)d\omega$ is the flux of electrons scattered into the solid angle $d\omega$,

θ is the angle between the paths of the scattered electrons and the incident electrons,

N is the number of molecules in the electron beam,

j_i is the flux of electrons in the incident beam crossing unit area,

and $Q(\theta)$ is the angular distribution of the scattered electrons and is called the scattering intensity function. It may be divided into three parts.

$$Q(\theta) = Q(s) = Q_{\text{atomic}}(s) + Q_{\text{molecular}}(s) + Q_{\text{incoherent}}(s) \quad (1b)$$

where $Q_{\text{at.}} = K^2 \sum_i F_i^2$, (1c)

$$Q_{\text{mol.}} = K^2 \sum_i \sum_{j \neq i} F_i F_j \frac{\sin r_{ij} s}{r_{ij} s} \exp(-\overline{\delta r_{ij}^2} s^2 / 2) , \quad (1d)$$

$$Q_{\text{inc.}} = K^2 \sum_i S_i / s^4 \quad (1e)$$

in which $K = 8\pi^2 m e^2 / h^2$, m and e are the electronic mass and charge respectively and h is Planck's constant;

$F_i = (Z - f) / s^2$, atomic scattering form factor for electrons;

$f = 4\pi \int_0^\infty |\psi(r)|^2 [(s \sin rs) / rs] r^2 dr$, atomic scattering

factor for x-rays, $\psi(r)$ is the atomic wave function;

$s = 4\pi(\sin\theta/2)/\lambda$, where λ is the DeBroglie wavelength of the electrons;

r_{ij} = distance between the i th and j th atoms in the molecules;

$\overline{\delta r_{ij}^2}$ = mean square of the change due to thermal vibration in the distance r_{ij} ;

S_{ij} = inelastic scattering function*.

Corresponding expressions can be written for the diffraction of electrons by crystals, films, liquids and amorphorous solids. These expressions are similar to the x-ray diffraction equations for corresponding media in which $a_e f_e \sqrt{(1 + \cos^2 \theta)}/2$ is replaced by $2(Z_i - f_i)/a_H s^2$ where a_e and a_H are the "radii" of the electron and the hydrogen atom.

Electron diffraction is a useful tool in structural chemistry, particularly in the determination of the structure of molecules in the gaseous state. Inspection of Equation (1) will show that, in theory, all of the interatomic distances in a molecule can be found; hence, the structure, i.e. the positions of the atoms in space, can be determined up to certain ambiguities. In practice, accordingly, the performance of an electron diffraction camera is judged by its ability to detect and measure accurately all the interatomic distances in the molecules investigated. The performance may better be discussed in terms of the detail, range, and accuracy of the measurements of the scattering function which can be made with the camera. If the observed data do not contain sufficient detail, long interatomic distances will be missed. The ability to recognize and separate the different distances increases with the range of the scattering parameter g over which the function is measured. Since the scattering decreases rapidly with g , the range of observation is limited usually by the absolute error of the measurements; and of course, these errors limit the reliability of the detection of weak terms in Equation (1). The absolute error or its effect can be reduced by increasing either the sensitivity of the observations or the magnitude of the observed function.

* This function has been tabulated for the incoherent scattering of atoms by L. Bewilogua².

The principle of the electron diffraction camera is relatively simple. The camera performs three functions: The generation of high-velocity electrons, the introduction of the diffracting material into the electron beam, and the recording of data from which Equation (1) can be obtained. Inspection of this equation shows that the camera must measure the wavelength of the electrons, the scattering angle, and the number of electrons scattered at each angle. The wavelength of the electrons is related to the velocity by the DeBroglie equation and can be selected by control of the velocity, the kinetic energy, or the momenta of the electrons. The scattering angle can be found by geometry. In the camera introduced by Wierl³, the angle is determined from three points: the electron source, the diffraction center, and a point on the recording surface. The angle may be found by other geometrical arrangements such as two points along the scattered beam when the incident electrons form a parallel beam of known direction. The scattered electrons can be measured either as a current or as a charge or by their effect on a photographic emulsion. Thus, the elements of the electron diffraction camera are a source of high velocity electrons, a collimator to control the divergence of the electron beam or the cross-section of the diffraction zone, a diffraction zone, and a recording device.

High velocity electrons are usually obtained by electrostatic acceleration of low energy electrons. The kinetic energy of the electrons can be determined from the accelerating potential and the initial energy of the electrons. There will be an uncertainty in the energy (and the wavelength) corresponding to the distribution of the initial electron velocities which is finite for all electron sources. The uncertainty of the

electron energies of practical sources is usually small enough that a velocity selector is unnecessary.

Since the geometric points and lines (or planes) required for the exact determination of the scattering angle cannot be realized in practice, there will be uncertainties in the measurement of the angle. The observed data will be a sum of overlapping theoretical functions and the fine details or resolving power of the data may be lost. The uncertainty of angle will be introduced by the size of the source, the divergence of the collimator, the thickness of the diffraction zone, and the resolving power of the recording device.

However, when the size of the source approaches a point and the divergence of the beam approaches zero, the number of electrons in the incident beam approaches zero, the intensity per area per solid angle having a natural upper limit. Furthermore, as the volume of the intersection of the beam and the scattering material approaches a point, the probability of scattering becomes negligible if the density of scattering material is not correspondingly increased. Thus, all the elements must have finite dimensions if the experiment is to be performed in a practical length of time. Since the relative effect of the absolute error of measurement of the number of electrons is decreased when more scattered electrons are observed, a compromise should be made between resolving power and intensity.

The conflict between resolving power and intensity arises in the experimental use of the camera as well as its design. If the number of molecules in the diffraction region is large, some electrons will be scattered more than once; on the other hand when the number is small the

probability of scattering is slight. A discussion of multiple scattering is necessary in the final analysis of the performance of an electron diffraction camera.

PERFORMANCE

It became evident in the introductory discussion that the theoretical scattering function cannot be reproduced exactly in any camera. Since the primary function of nearly all electron diffraction experiments is the determination of the structure of molecules, the performance of an electron diffraction camera is evaluated from the detectability, separability, and accuracy of measurement of the interatomic distance terms in the recorded scattering function. However, all these qualities are not expressed explicitly in the observed scattering function. Since the Fourier transform of a scattering function is related to the distribution of interatomic distances, it is reasonable to expect that the detectability and separability will be recognized easily in the transform of the altered scattering function; and indeed, it will be shown later that this conjecture is true.

The Fourier transform $F(r)$ of the function $f(s)$ is defined by the integral

$$F(r) = 1/\sqrt{2\pi} \int_{-\infty}^{\infty} f(s) \exp(irs) ds$$

and is connected to the sine and cosine transforms

$$\begin{aligned} F_s(r) &= 1/\sqrt{2\pi} \int_{-\infty}^{\infty} f(s) \sin(rs) ds = -i/2 [F(r) - F(-r)] \\ \text{and } F_c(r) &= 1/\sqrt{2\pi} \int_{-\infty}^{\infty} f(s) \cos(rs) ds = 1/2 [F(r) + F(-r)] \end{aligned} \quad (2)$$

by the relations

$$F(r) = \begin{cases} (F_c(r) + iF_s(r)) * \\ (F_c^2 + F_s^2)^{\frac{1}{2}} \exp [i \tan^{-1}(F_s/F_c)] \\ |F(r)| \exp [i\phi(r)] \end{cases}$$

Since the transform of a sum is the sum of the transforms of the parts, each interatomic distance term can be treated separately. The transform of a term in the theoretical scattering function or some modification of it, such as the visual intensity function (theoretical), represents the ideal of performance. When this transform is compared with that which is obtained from a correspondingly modified observed diffraction pattern, the performance may be estimated from the dissimilarity.

The camera alters the theoretical scattering function in two ways. First, an indeterminacy is introduced into the observation of the scattering angle. Second, the intensity of scattering is modified by a factor which is a function of the scattering angle; in particular, the pattern is recorded only in a finite range.

* Some other properties of Fourier transforms which will be used are:

- 1) The inverse transform is $f(s) = 1/\sqrt{2\pi} \int_{-\infty}^{\infty} F(r) \exp(-irs) dr$.
- 2) The transform of an even, real function is even and real.
- 3) The transform of an odd, real function is odd and imaginary.

Indeterminacy of the scattering angle. If there are uncertainties in observing the scattering angle, the observed scattering function will consist of superimposed theoretical functions. Consider that the theoretical function, $\mathcal{Q}(s)$, is defined by the equation

$$\mathcal{Q}(s) = \int_{-\infty}^{\infty} \mathcal{Q}(t) \delta(s-t) dt \quad (3)$$

The unit impulse or δ function, $\delta(s-t)$, is a singular and an improper function having the value zero when $s \neq t$ and presenting a unit area. Due to an uncertainty in s (or θ) each unit impulse is spread out into a function which still presents a unit area but is no longer improper. Such functions will be called spreading functions and will be designated by $g(s-t, t)$. Thus, the observed function will be

$$\mathcal{Q}_o(s) = \int_{-\infty}^{\infty} \mathcal{Q}(t) g(s-t, t) dt \quad (4)$$

the folding of \mathcal{Q} with g . (Folding is a commutative operation.) When a second uncertainty is introduced, \mathcal{Q}_o is folded with the second spreading function, $g_2(s-t, t)$, and similarly for all the other uncertainties.

The spreading functions may be classified according to the form of the variable $(s-t, t)$. Two classes are sufficient to discuss approximately the spreading functions encountered in a camera design.

Class I spreading functions. If the spreading function has a width parameter which is independent of the scattering angle, it may be written as $g(s-t)$. In treatises on Fourier transforms, it will be found that the transform of

$$\int_{-\infty}^{\infty} f_1(t) \cdot f_2(s-t) dt \quad (5)$$

$$F_1(r) \cdot F_2(r) \quad ,$$

is:

where $F_{nI}(r)$ is the transform of $f_{nI}(s)$. Hence, the transform of

$$I_0(s) = \int_{-\infty}^{\infty} I(t) g_{I}(s-t) dt \quad (6)$$

is $D_0(r) = D(r)G_{I}(r) = D(r)|G_{I}(r)| \exp[i\gamma(r)]$,

where $D(r)$, which is real, is the transform of $I(s)$, and $G_{I}(r)$, which may be complex*, is the transform of $g_{I}(s)$. Successive application of Equation (6) for each independent spreading function gives

$$G_{tI}(r) = G_{I 1,2,3\dots}(r) = G_{I 1}(r)G_{I 2}(r)G_{I 3}(r)\dots\dots\dots \quad (7)$$

$$= \prod_i |G_{I i}(r)| \exp\left[i \sum_i \gamma_i(r)\right]$$

Class II spreading function. If the width of the spreading function is proportional to the scattering parameter s , the observed scattering function will be

$$I_0(s) = \int_{-\infty}^{\infty} \frac{I(t)}{t} \cdot g_{II}\left(\frac{ss-t}{t}\right) dt \quad (8)$$

It is shown in Appendix I that the transform of this integral is

$$D_0(r) = \int_{-\infty}^{\infty} I(t) \cdot G_{II}(rt) \exp(irt) dt \quad (9)$$

$$= \int_{-\infty}^{\infty} \frac{D(p)}{r} \cdot G_{II}\left(\frac{p_0-r}{r}\right) dp \quad (10)$$

That is to say, the transform of a spreading function of Class II folded with the theoretical scattering function is a kind of folding of g_{II} with the theoretical distribution functions. When there are more than one spreading function of this class, Equation (9) becomes

* The spreading functions are positive (and real) for all values of s . Therefore, they always contain an even component whose transform is real and may contain an odd component whose transform is imaginary.

$$D_o(r) = \int_{-\infty}^{\infty} Q(t) \cdot G_{t_{II}}(rt) \exp(irt) dt \quad , \quad (11)$$

where $G_{t_{II}}(rt) = G_1(rt)G_2(rt)G_3(rt)\dots$, and the transform will be

$$D_o(r) = \int_{-\infty}^{\infty} \frac{D(p)}{r} \cdot g_{t_{II}}\left(\frac{p-r}{r}\right) dp \quad , \quad (12)$$

where $g_{t_{II}}$ is the transform of $G_{t_{II}}$.

The form of the spreading function. Even when the exact form of all the spreading functions and their transforms are known, it is practical to make a limited number of approximations. In the problem at hand two approximations selected for their simplicity of form and interpretation appear to be adequate.

Approximation 1. The unit impulse is spread into a Gaussian error distribution

$$g_1(x) = (1/w\sqrt{2\pi}) \exp(-x^2/2w^2) \quad (13)$$

whose transform is $G_1(y) = (1/\sqrt{2\pi}) \exp(-w^2y^2/2)$.

Here w is the standard (quadratic mean) deviation of the distribution and the products in Equations (7) and (11) are simply

$$G_{t_1}(y) = (1/\sqrt{2\pi}) \exp(-(w_1^2 - w_2^2 - w_3^2 - \dots)y^2/2) \quad (14)$$

Approximation 2. The unit impulse is spread uniformly and symmetrically over the interval $2w$

$$g_2(x) = \begin{cases} 1/2w, & \text{when } |x| \leq w \\ 0, & \text{when } |x| > w \end{cases} \quad (15)$$

and the transform is $G_2(y) = (1/\sqrt{2\pi})(\sin wy)/wy$.

The meaning of the half-width w is evident, but unfortunately, the transform G_2 does not lend itself to convenient application of Equations (7) and (11). Equations (15) may be approximated by Equations (13) if w' equals the standard deviation of g_2 which is $w' = w/\sqrt{3}$. That is,

$$\left. \begin{aligned} g_2(x) &\approx \left[(\sqrt{3/2\pi})/w \right] \exp(-3x^2/2w^2) \\ G_2(y) &\approx (1/\sqrt{2\pi}) \exp(-w^2 y^2/6) \end{aligned} \right\} \quad (15a)$$

and

$$G_{t_2}(y) \approx (1/\sqrt{2\pi}) \exp[-(w_1^2 + w_2^2 + w_3^2 \dots) y^2/6] \quad (16)$$

Within the range that the approximate transform is used, the maximum error is about 3% when only one spreading function is dominant. When several spreading functions, whose half-widths are approximately equal, dominate, the error decreases rapidly.

The uncertainty of g_s may be due either to a distribution of the electron energies or to an indeterminacy in the geometry of measuring the scattering angle. If the electron energies are spread from $eE - e\Delta E$ to $eE + e\Delta E$, where eE is the potential through which the electrons have been accelerated,

then

$$\lambda \pm \Delta\lambda = h/\sqrt{2me(E \pm \Delta E)} \approx \lambda(1 \pm \Delta E/2E),$$

and

$$2w_{\pm} = (s_+ + w) - (s_- - w) = (4\pi/\lambda) \sin(\phi/2) \left\{ \frac{\Delta E}{E(1 - \Delta E^2/4E^2)} \right\},$$

hence

$$w_{\pm} \approx -s \Delta E/2E. \quad (17)$$

If the angle is indeterminate between $\phi - \Delta\phi$ and $\phi + \Delta\phi$,

$$2w_{\pm} = (4\pi/\lambda) \left[\frac{\sin(\phi + \Delta\phi)}{2} - \frac{\sin(\phi - \Delta\phi)}{2} \right]$$

and

$$\begin{aligned} w_{\pm} &= (4\pi/\lambda) \cos(\phi/2) \sin(\Delta\phi/2) \\ &\approx (2\pi/\lambda) \cos(\phi/2) \Delta\phi. \end{aligned} \quad (18)$$

Modification of the intensity. The camera also modifies the theoretical scattering function by a factor which depends on the scattering parameter; that is,

$$D_0(s) = D(s) m(s) \quad (19)$$

The transform of this modified function is

$$D_0(r) = \int_{-\infty}^{\infty} D(p) M(r-p) dp \quad (20)$$

where $M(r)$ is the transform of $m(s)$.

The most important modification is that due to the finite range over which the diffraction pattern may be observed, for which $m(s)$ is

$$m(s) = \begin{cases} 1, & |s| \leq s_m \\ 0, & |s| > s_m \end{cases} \quad (21)$$

and the transform is

$$M(r) \begin{cases} = (1/\sqrt{2\pi}) \sin(s_m r)/r \\ \approx (s_m/\sqrt{2\pi}) \exp(-s_m^2 r^2/6) * \end{cases} \quad (22)$$

The limit of observation cannot be made arbitrarily large by the simple expedient of increasing the range of recording by the camera. There will still be a maximum value of the parameter s beyond which observations of the scattering function are meaningless. This limit is reached for a particular interatomic distance when the uncertainty of measurement equals the amplitude of the corresponding term in Equation (1) as altered by the camera and multiple scattering. If N is the number of molecules in the diffraction zone, t is the duration of the experiment, and ΔQ is the uncertainty in the measurement of the charge scattered into the solid angle $d\omega$, then s_m

* When this approximate transform is used, then

$$m(s) = (\sqrt{3/2\pi}) \exp(-3s^2/2s_m^2) \quad (21a)$$

is determined by the equation

$$Nt j_i k^2 \mathcal{O} \left\{ \frac{[Z - f(s_m)]_i [Z - f(s_m)]_j}{r_{ij} s_m^2} \right\} d\omega = \Delta Q_{\min} \quad (23)$$

where $\mathcal{O}\{\}$ describes the change produced in the amplitude of $F_i F_j \sin(r_{ij} s) / r_{ij} s$ by the camera and multiple scattering. The magnitude of the operator $\mathcal{O}\{\}$ is one for the unaltered function, but it is less than one and is a function of r_{ij} and s in any camera. It is clear that s_m , the limit of observation, can be extended by increasing either the sensitivity of the measurement, $1/\Delta Q_{\min}$, or the duration of the observation. It also appears that s_m increases with the factors N , j_i , $\mathcal{O}\{\}$, and $d\omega$; but it will be seen shortly that these factors are not independent. In particular, $\mathcal{O}\{\}$ decreases as N , j_i , and $d\omega$ are increased.

The number of molecules in the diffraction zone is

$$nV = n \bar{C} \bar{l} \quad (24)$$

where n is the number of molecules per unit area, V is the volume of the scattering zone, \bar{C} is the average cross-section, and \bar{l} is the average length. The indeterminacy of the scattering angle increases with the volume of the diffraction zone; hence, if the density of scattering matter is held constant, s_m does not become arbitrarily large with $V = \bar{C} \bar{l}$ since the indeterminacy reduces the magnitude of the operator $\mathcal{O}\{\}$. Also, the number of molecules per unit volume n cannot be increased without limit, and even before a condensed phase is obtained multiple scattering will have masked the desired scattering pattern by spreading.

The upper limit of the current density j_i of the electron beam is a function of the specific emission of the source and the angle of divergence of the beam.

$$j_m = j_0 \left(1 - \frac{eE}{kT}\right) \sin^2 \alpha = j_0 \left(1 - \frac{11600E}{T}\right) \sin^2 \alpha \quad (25)$$

where j_m is the maximum current density in the beam,

j_0 is the specific emission of the cathode,

E is the accelerating potential,

T , is the cathode temperature,

k is Boltzmann's constant,

and α is the half angle of divergence or convergence.

This expression is a consequence of the second law of thermodynamics and corresponds to the theorem of Helmholtz-Lagrange in optics. It was derived by D. B. Langmuir⁴ in the above form for electron beams and takes into account the Maxwellian velocity distribution of the electrons leaving the source. The choice of the cathode material and the upper limit of the operating temperature are dictated by practical considerations and determine the specific emission of the source. The only factor in the camera design controlling the current density is the divergence of the beam. Therefore, the maximum current density in the diffraction zone is determined by the apparent angle subtended by the source at the diffraction center. This angle is an uncertainty in the scattering angle and the current density cannot be increased beyond the limit of Equation (25) without reducing the magnitude of θ .

The solid angle $d\omega$ may be written

$$d\omega = \sin \theta d\theta d\phi = (\lambda/2\pi) s \cos(\theta/2) d\theta d\phi \quad (26)$$

$$\Delta\omega \approx (\lambda/4\pi) s \cos(\theta/2) \Delta\theta_r \Delta\phi_r$$

$\Delta\theta_r$ is the azimuthal arc of the diffraction pattern and $\Delta\phi_r$ is the arc

of the scattering angle intercepted by the recording device. $\Delta \theta_r$ cannot exceed 2π . $\Delta \theta_r$ is another uncertainty in the scattering angle and reduces $|O\{\}\rangle$.

It should not be forgotten that ΔQ_{\min} is a function of the total charge Q_t which is being measured. ΔQ_{\min} usually becomes constant as the total charge approaches zero. For large Q_t the ratio $\Delta Q_{\min} / \Delta Q_t$ is nearly constant.

The complete expression for the transform of the approximate observed scattering function. Combining Equations (6), (8), and (19) gives for the observed scattering function:

$$D_o(s) = \int_{-\infty}^{\infty} g_{It}(s-t) \int_{-\infty}^{\infty} \frac{D(t')m(t')}{t'} g_{II t'}\left(\frac{t-t'}{t'}\right) dt' dt \quad (27)$$

whose transform is:

$$D_o(r) = G_{It}(r) \int_{-\infty}^{\infty} D(t')m(t') G_{II t'}(rt') \exp(irt') dt' \quad (28)$$

Upon substitution of the approximations made in Equations (16) and (21a), Equation (28) may be written:

$$D_o(r) = \exp\left(-\frac{\sum w_{II}^2 r^2}{6}\right) \frac{s_m}{\sqrt{1 + \sum (w_{II} r s_m / 3)^2}} \times \int_{-\infty}^{\infty} D(p) \exp\left(\frac{-s_m^2 (r-p)^2}{6[1 + \sum (w_{II} r s_m / 3)^2]}\right) dp \quad (29)$$

This expression should also include a term due to experimental errors in recording of the scattering pattern.

Inspection of Equation (29) will reveal that the alteration of the theoretical distribution is described by the two functions

$$\exp\left(-\frac{\sum w_{II}^2 r^2}{6}\right) \quad \text{and} \quad \frac{s_m}{\sqrt{1 + \sum (w_{II} r s_m / 3)^2}} \quad (30)$$

Their product modifies the amplitude of the theoretical distribution and should be large with respect to the error term, otherwise it will be difficult to detect an interatomic distance. When there are more than one interatomic distance, the observed distribution may be smeared out sufficiently by the folding in Equation (29) that the error term makes separate identification of two or more adjacent distances uncertain*. The limit of separability $(\Delta r)_L$ is proportional to the width of the Gaussian function in the integrand of Equation (29),

$$(\Delta r)_L = \sqrt{6} k_s \left(\frac{\sqrt{1 + \sum (w_{II} r s_m / 3)^2}}{s_m} \right) \quad (31)$$

which is inversely proportional to one of the alteration functions (30).

The product

$$\left(\frac{s_m}{\sqrt{1 + \sum (w_{II} r s_m / 3)^2}} \right) \exp\left(-\frac{\sum w_{II}^2 r^2}{6}\right) \quad (32)$$

is a measure of the merit of a camera design, since the greater its magnitude the more readily interatomic distance terms can be detected and separated. s_m , w_I , and w_{II} cannot be varied independently but are functions of the dimensions of the camera elements. In order to evaluate s_m it is necessary to know $|\theta\{\}\rangle$. This function has a simple form only when $\mathcal{Q}(s)$ is a sum of sines and cosines. In this case reinversion of Equation (28) gives:

* When at least one of the adjoining distances has a large temperature factor, the determination of the separation is still less certain.

$$D_0(s) = O\{D(s)\} = G_{It}(r_{ij})G_{II}(r_{ij}s)m(s)D(s) \quad (33)$$

and the approximation will be made that

$$O\{\} \approx \exp\left(-\frac{\sum w_{Ij}^2 r_{ij}^2}{6}\right) \exp\left(-\frac{\sum w_{IIj}^2 r_{ij}^2 s^2}{6}\right) \quad (1) \quad (34)$$

Unless the widths of the spreading functions g_I and g_{II} become large with respect to the period of $\sin(r_{ij}s)$, this approximation should be satisfactory.

Accuracy. The alteration of the scattering function by the camera may introduce systematic errors which either introduce asymmetries into or shift the inflections* in the distribution function $D_0(r)$, thus leading to an inaccurate determination of the distances. These errors arise (1) from an odd term in the spreading function, (2) from the slope of the transform G_{It} , and (3) from the actual asymmetry of $g_{II}(\frac{r-D}{r})$. The first-order effect of an odd term in a spreading function is removed if the g scale is calibrated to coincide with the centers of gravity of the spreading function**. Higher order effects would require separate g scales for each interatomic distance.

Transforms of modified scattering functions. The differences between the transforms $D(r)$ and $D_0(r)$ describe the alteration by the camera of the theoretical scattering function $D(s)$ to $D_0(s)$. However, in nearly all electron diffraction determinations a related function such as the observed visual scattering function is used instead of $D(s)$. Hence, it

* Each of the coherent scattering terms in $D(s)$ is represented by an inflection in $D(r)$ at $r = \frac{1}{s} r_{ij}$.

** Such a calibration can be made if the g scale is determined from the individual lines of the diffraction pattern of a crystal of known spacing.

is more appropriate to describe the changes in the related function by means of its own transform.

The radial distribution function used in this laboratory is the transform of $sI_0(s)$

$$rD_0(r) = (1/\sqrt{2\pi}) \int_{-\infty}^{\infty} sI_0(s) \exp(irs) ds \quad (35)$$

$I_0(s)$, the observed visual scattering function, is $Q_0(s)$ modified by the physiological response of eye and by interpretation. This modification can be described approximately by the relation

$$I_0(s) = v_0(s) [Q_0(s) - Q_B(s)] \quad (36)$$

where Q_B is the background subtracted by the eye, and v_0 represents the change in sensitivity of the eye with the background and is approximately equal to $1/Q_B(s)$ over a large range. Equation (35) may then be written

$$rD_0(r) = -\frac{\partial}{\partial r} d_0(r) = -\frac{\partial}{\partial r} \int_{-\infty}^{\infty} [D_0(p) - D_B(p)] \mathcal{V}(r-p) dp \quad (37)$$

where $d_0(r)$ is the transform of $I_0(s)$ and $\mathcal{V}(r)$ is the transform of $v_0(s)$. To find the difference between $rD_0(r)$ and $rD(r)$, it is necessary to substitute $D_0(p)$ from either Equation (28) or (29) and make suitable approximations for D_B , $\mathcal{V}(r-p)$, and the relation between $D(r)$ and $rD(r)$. Although a complete understanding of the alteration of $rD(r)$ to $rD_0(r)$ requires the analysis indicated, investigation of the approximations needed has not been undertaken since Equations (28) and (29) describe this alteration to a first-order approximation, which is adequate for the design of a camera.

COMPONENTS OF AN ELECTRON DIFFRACTION CAMERA

The components of an electron diffraction camera are a source of nearly monokinetic electrons, a collimator, a diffraction zone and a recording device. In this section the purpose and general principles of operation of each component is given. The relation of the dimensions to the intensity factor $N_j d\omega / A Q_{\min}$ in Equation (23) is evident with the aid of Equations (24) and (25). The connection between the sizes of the components and the widths of the spreading functions is shown in later sections.

The monokinetic electron source. Electrons for diffraction have been obtained either from a gas discharge tube or from a thermionic cathode. The thermionic cathode has replaced almost universally the gas discharge tube because it is easier to control and because the uncertainty of the initial electron energies is much smaller. The choice of cathode material and operating temperature affects both the detectability and separability. The specific emission of thermionic emitters is given by the Richardson-Dushman⁵ equation,

$$j_0 = BT^2 \exp(-W/kT) \quad , \quad (38)$$

where j_0 is the specific emission of the cathode,

B is a constant ($= 60.2$ for tungsten),

W is the thermionic electron work function ($= 4.52$ volts for tungsten),

and k is Boltzmann's constant ($= 8.63 \times 10^{-5}$ electron volt/degree).

The distribution of electrons emitted from a thermionic cathode follows the

Maxwellian law. Let $\chi(E)dE$ be the fraction of electrons emitted with initial energy between eE and $e(E + dE)$; then

$$\chi(E)dE = (e/kT)^2 \cdot \exp(-eE/kT) \cdot E \cdot dE \quad (39)$$

This distribution has a maximum at $E_m = kT/e = T/11,600$ volt and 90% of the electrons have energies less than $4kT/e$. If the temperature of the cathode is 2900°K ., E_m is 0.25 volt and the half width of the spreading function for the initial electron velocities is approximately

$$W_{1/2} = - \frac{3kT}{eE_{\text{accelerating}}} = - 6.25 \times 10^{-6} \text{ s} \quad (40)$$

(Cathode temperature = 2900°K .; accelerating potential = $40,000$ volts)

It will be seen later that this spreading is negligible compared with that from other causes and that the choice of emission temperature is not critical. Thus, the selection of an emitter need not be based on a low operating temperature. Instead, it appears that a better choice can be made on the grounds of the specific emission at a temperature such that cathodes of different emitters would have the same mean-lives. If short lives, of the order of ten hours, can be tolerated (by the use of readily interchangeable cathodes), tungsten would be selected on this basis alone. Further, tungsten has the important advantage that contamination from the air and from the materials studied in the camera has a small effect on the emission in comparison with the effect on oxide-coated and thoriated-tungsten cathodes.

After emission the electrons are accelerated by an electrostatic field which is produced by a high potential applied between the cathode and anode (accelerating electrode). Changes in the accelerating potential from one

exposure to another will result in different g scales for the separate experiments. Thus, if the g scale is to be reliable to one part in a thousand, the voltage must be reproducible to one part in five hundred. On the other hand, variation of the accelerating potential during an exposure is a spreading function. If the voltage during an exposure is held to one part in five hundred, the half width of the spreading function will be

$$w_2 = 10^{-3} \text{ sec.} \quad (41)$$

The intensity and size of the electron source can be controlled by the design of the cathode, anode, and other electrodes in the field between them within the limits of Equation (25). This group of electrodes form an electron lens system, and either the image of the cathode or the pupil (cross-over in the formation of the image) is the effective source in the camera geometry. The effective size of the source cannot be made much smaller than 10^{-2} millimeter.

The current density in the beam at the diffraction zone depends greatly on the design of the electromagnet. About 25% of the theoretical current density predicted by Equation (25) is realized in a good design.

The collimator. The collimator controls the divergence and the cross-section at the diffraction zone of the electron beam. It may consist of one or more apertures or pinholes which may be placed ahead or behind the diffraction zone along the electron beam and limit the divergence of the undiffracted or the diffracted beam or both. In many of the electron diffraction cameras pinholes are used for collimation. In the same way that ordinary optical systems make more efficient use of light when lenses are used instead of pinholes, electron lenses may be used to a certain

extent in electron diffraction to increase the electron intensity without loss of detail in the scattering pattern. Such systems are discussed later.

The diffraction zone. In the usual methods of diffraction of electrons, a thin section of a solid specimen or a fine jet of gas is introduced perpendicular to the electron beam. When gases are studied the length of the diffraction zone (diameter of the jet) cannot be made significantly smaller than one millimeter. At wide angles this uncertainty in the scattering angle becomes the most important contribution to the spreading of the scattering pattern in existing cameras. This uncertainty in the scattering angle is approximately proportional to the ratio of the diameter of the jet to the camera length (distance between the diffraction center and the recording device). An ideal lens between the diffraction zone and the recording device can be focused so that the apparent camera length increases without limit and decreases the uncertainty in the scattering angle. Such a gain in performance is limited and perhaps is not even realized when practical lenses with their aberrations are used.

The recording device. The pattern of the scattered electrons is recorded almost universally on photographic films. The selection of emulsions for electron diffraction of gases has been empirical and represents a compromise among the film characteristics, speed, resolving power, and latitude. The relation of the film characteristics to performance will not be analyzed here. In the application of the results of this discussion to photographic recording, it will be assumed that the effect of the resolving power of the emulsion may be neglected and that the speed and latitude are adequate. The resolving power is the most important of these

parameters. The sensitivity (reciprocal of the minimum uncertainty in the recording of the scattered charge) can be made equal for all emulsions by selection of an appropriate exposure (product of the intensity of the scattered electron and the duration of the experiment*). When the latitude of the film is limited, the complete pattern can be obtained from a series of graded exposures, each covering a portion of the pattern**.

The diffraction patterns of solids have been recorded by electrical measurement of scattered charges or currents, but no applications of this method of recording to the scattering of gases have been reported***.

The relation between sensitivity and the size of probe is evident from Equation (23). If the angular size of the probe is $\Delta\phi \cdot \Delta\theta$, then

$$\Delta\omega \approx \sin\phi \cdot \Delta\phi \cdot \Delta\theta \approx \left(\frac{\lambda}{2\pi}\right)^2 \Delta\phi \cdot \Delta\theta, \quad (42)$$

while the half-width of the spreading function is

$$w_{\frac{1}{2}} \approx (2\pi/\lambda) \cos(\phi/2) \Delta\phi. \quad (43)$$

* If the system is stable, adequate exposure can be obtained by lengthening the time of the experiment. Such stability has not yet been demonstrated in cameras used for the diffraction of electrons by gases; the length of an experiment is limited to a fraction of a second. However, the effective length of an experiment can be further increased by superimposing on one film a series of short experiments. Since this is a tedious process, speed should not be sacrificed to resolving power any farther than necessary.

** Provided that the segment of the pattern covered by a single experiment is not so narrow that adjoining features cannot be compared.

*** This is due in part to the failure to devise a satisfactory technique and in part to the great success and sensitivity of the photographic method. In a later section the theoretical limitation of electrical measurement of the scattering pattern is investigated.

GEOMETRIC THEORY OF DIFFRACTION

All of the components of the electron diffraction camera introduce geometric uncertainties into the scattering angle. These uncertainties were not discussed quantitatively along with the description of the individual components since the whole problem of geometric uncertainty is discussed better as a unit. In the geometric theory, the spreading of the scattering function due to the effective size of the source, the divergence of the electron beam, the length of the diffraction zone, and the shape of the recording surface will be treated.

First-order geometric theory of diffraction. Diffraction has certain quasi-optical properties. In analogy with optical theory, an image surface, magnification, and aberrations can be defined. When electrons diverging from a source or image are diffracted, there is a virtual image for each scattering angle, and when electrons converging to a real image are diffracted, the images are real. The diffraction image with its aberrations may be focused by electron lenses.

The focusing circle used in some spectrographs is familiar. In a first approximation a spherical surface possesses the same focal property. Consider an electron ray pencil converging or diverging at the point P . Locate the diffraction center O on the principal ray and construct a sphere whose diameter is PO , see Figure 1. If the diffraction region is a thin spherical shell at the surface of this sphere, the diffracted ray pencil will be inclined at an angle ϕ and will be convergent at or divergent from the point P' with

$$P'O = PO \cos \phi$$

and $\sin \beta' = \sin \beta$.

Let a second ray pencil, convergent at R , also on the surface, be diffracted.

The second diffracted ray pencil will be convergent at R' and

$$R'P' = RP$$

and $\angle R'OP' = \angle ROP$.

These results describe the first-order approximation of diffraction.

Second-order geometric theory of diffraction. In the diffraction of electrons by gases it is impossible to confine the gas in the diffraction zone to a thin spherical shell. The shape of the diffraction zone is more simply described by a succession of planes. By considering first that the diffracting material lies in a plane, aberrations from the first-order image can be found in a second-order approximation. Then by treating diffraction from successive planes, first-order uncertainty will be found.

Let the Z axis be the axis of the system, i.e. passing through the centers of the source, the collimating aperture, the diffraction zone, and the recording surface; and place the origin at the diffraction center as in Figure 2. In the second-order approximation consider only the rays which lie (both before and after diffraction) in a plane containing the Z axis. The distance of the ray from the Z axis is R . The source is placed at P and the collimating aperture at A . The ideal image point is defined by the ray R_1 from a point source at P , passing through a point aperture and diffracted at the origin; its path is

$$R_1 = \begin{cases} \text{zero} & (\text{incident}) \\ Z \tan \phi & (\text{diffracted}) \end{cases} \quad (44)$$

An arbitrary ray R_2 , originating at R_p and passing through the aperture at R_A and diffracted at R_0 , makes an angle γ with R_1 . Its path is

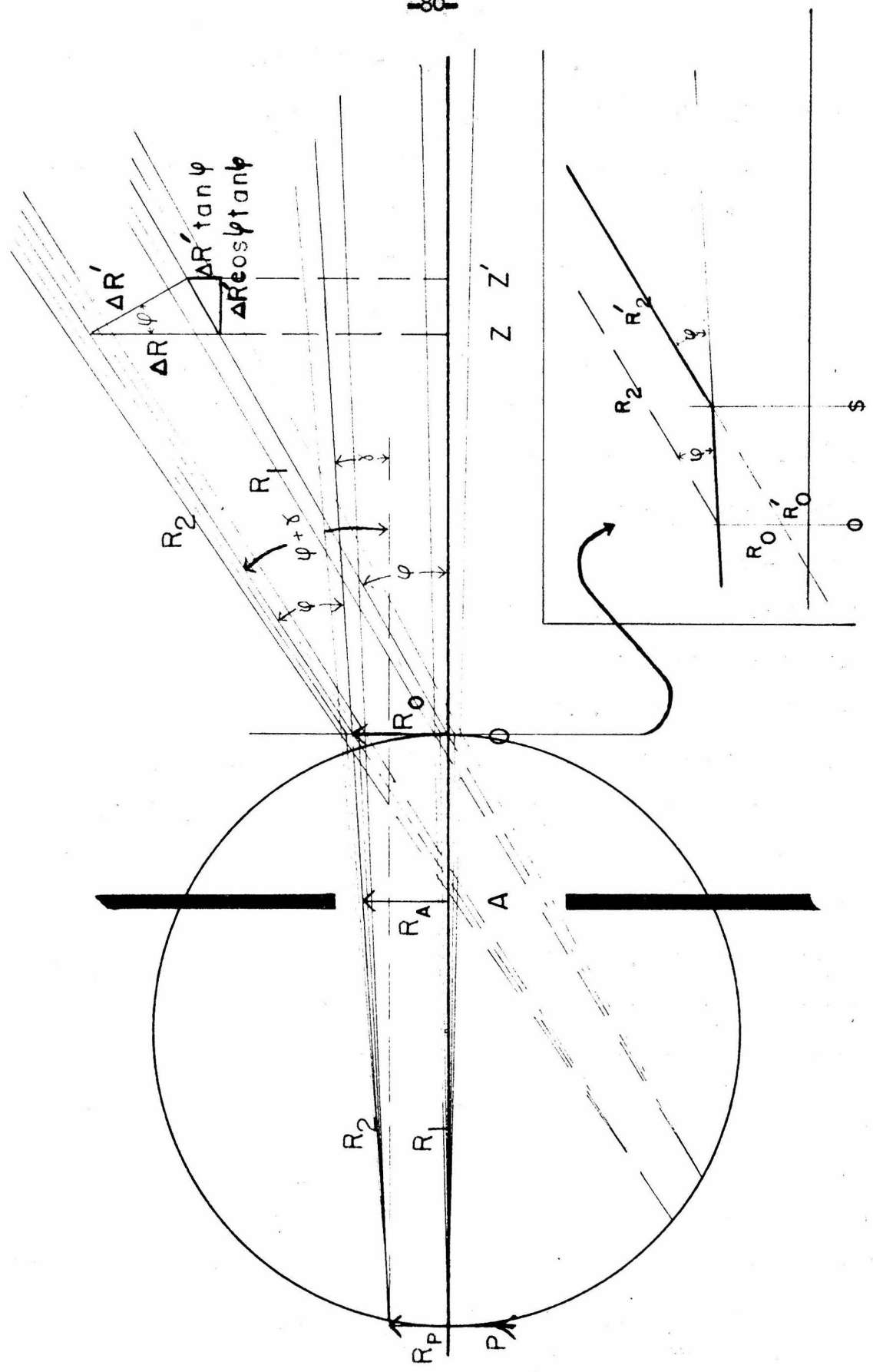


Figure 2

$$R_2 = \begin{cases} R_0 + Z \tan \gamma & \text{(incident)} \\ R_0 + Z \tan(\phi + \gamma) & \text{(diffracted)} \end{cases}, \quad (45)$$

and the difference between the diffracted paths is

$$\Delta R = R_2 - R_1 = R_0 + Z [\tan(\phi + \gamma) - \tan \phi] \quad (46)$$

The tangent of the angle subtended by ΔR is

$$\begin{aligned} \tan \Delta \phi &= \Delta R / Z' \sec \phi \\ &= \frac{R_0 + Z [(\tan \gamma \sec^2 \phi) / (1 - \tan \gamma \tan \phi)]}{Z' \sec^2 \phi}, \end{aligned} \quad (47)$$

but $Z = Z' - \Delta R \sin \phi = Z'(1 - \tan \Delta \phi \tan \phi)$

Thus $\tan \Delta \phi = \frac{R_0 \cos^2 \phi}{Z'} + \frac{\tan \gamma (1 - \tan \phi \tan \Delta \phi)}{1 - \tan \gamma \tan \phi}$

Solving for $\tan \Delta \phi$ it is found that

$$\tan \Delta \phi = \frac{R_0}{Z' \sec^2 \phi} (1 - \tan \gamma \tan \phi) + \tan \gamma \quad (48)$$

Expressing the parameters R_0 and $\tan \gamma$ in terms of R_P and R_A

$$R_0 = (PR_A - AR_P) / (P - A)$$

$$\tan \gamma = (R_P - R_A) / (P - A)$$

and substituting in Equation (48), then

$$\tan \Delta \phi = \frac{(Z' \sec^2 \phi - A)R_P}{(P - A)Z' \sec^2 \phi} - \frac{(Z' \sec^2 \phi - P)R_A}{(P - A)Z' \sec^2 \phi} - \frac{R_0 \tan \phi \tan \gamma}{Z' \sec^2 \phi} \quad (49)$$

The term $\frac{Z' \sec^2 \phi - A}{(P - A)Z' \sec^2 \phi} R_P$ describes the ideal image in which $\frac{P(Z' \sec^2 \phi - A)}{(P - A)Z' \sec^2 \phi}$

is the angular magnification. $\frac{(Z' \sec^2 \phi - P)R_A}{(P - A)Z' \sec^2 \phi}$ is the defocusing term and

is zero on the ideal image surface;

$$Z' = P \cos^2 \phi \quad (50)$$

The second-order term, $R_0 \tan \delta \tan \phi / Z' \sec^2 \phi$, describes the aberrations resulting from a plane diffraction surface. Expanding $R_0 \tan \delta$ the angular half-width becomes

$$\tan \Delta \phi = \frac{\tan \phi}{2Z'(P-A)^2 \sec^2 \phi} \left[FR_A^2 - (P-A)R_P R_A - AR_P^2 \right] \quad (51)$$

in which the radii of the source and of the collimating aperture are used for R_P and R_A respectively.

To find the effect of the length of the diffraction zone, consider a ray R_2^1 diffracted at the plane $Z = S$. It is evident that R_2^1 is identical with a ray R_2 for which R_0^1 is substituted for R_0 (see Figure 2, inset)

$$\begin{aligned} R_0^1 &= R_0 - (R_0 - R_0^1) = R_0 - S [\tan(\phi - \gamma) - \tan \gamma] \\ &= R_0 - (S \tan \phi \sec^2 \gamma) / (1 - \tan \phi \tan \gamma) \end{aligned}$$

Substituting in Equation (49)

$$\tan \Delta \phi = \tan \Delta \phi_{S=0} - S \tan \phi \sec^2 \gamma / Z' \sec^2 \phi \quad (52a)$$

Thus the uncertainty due to the length of the diffraction zone is

$$\tan \Delta \phi = S \sec^2 \gamma \sin \phi \cos \phi / Z' \quad (52b)$$

in which half the mean length of the diffraction zone is used for S .

ELECTRON LENSES AND THEIR APPLICATION TO ELECTRON DIFFRACTION

Electrons can be focused by electric and magnetic fields. It is predicted from the first-order theory of lenses that most of the geometric uncertainties* in the scattering angle can be decreased without limit regardless of the dimensions of the components of the camera. However, the higher order lens theory shows that the nearly ideal performance, predicted by the first-order theory, will not be realized since practical lenses introduce new uncertainties (aberrations) which generally are smaller than those present in the absence of lenses except at large angles.

Lens aberrations. The theory of the aberrations of electron lenses has been discussed by several authors⁶. The treatment of Rogowski as outlined by Zworykin et al⁷ will be followed here appropriately modified for radial symmetric images. In contrast to the exact ray tracing methods used in the careful design of ordinary optical systems, it is sufficient to describe the aberrations by the coefficients of the second lowest order terms in ray equations since these aberrations cannot be corrected sufficiently to make any higher order aberrations become important.

The aberrations of electron lenses are usually divided into three groups: (1) geometric aberrations which depend on the geometry of the lens fields, (2) chromatic aberrations which arise from the inhomogeneity of the electron velocities, and (3) space charge effects which are produced by the mutual repulsion of the electrons and depend on the electron density.

Geometric aberrations. The ray equation for axial symmetric lenses contains only odd order terms. The first-order terms define the ideal or

* All but the uncertainty due to the finite size of the elements of the recording device.

Gaussian image while the third-order terms describe the most important aberrations. If the axial symmetric lens is isotropic, there are five aberrations (distortion, curvature of field, astigmatism, coma, and spherical aberration) as in ordinary optics. However, magnetic fields are non-isotropic and three additional aberrations arise in this case (anisotropic distortion, astigmatism and coma). The characteristic aberration figures can be described easily in the Gaussian (ideal) image plane by eight aberration coefficients.

Let (R_p, θ') be the coordinates of a point in the object plane,

(R_A, ψ) be the coordinates of the intersection of a ray in the aperture plane,

(R_I, θ) be the coordinates of the aberrationless (Gaussian) image of (R_p, θ') in the image plane and let $\theta = 0$ be parallel to $\psi = 0$,

$(\Delta R, \Delta \theta)$ be the deviation of the ray from the Gaussian image point,

$\theta - \theta' = \chi$ be the angle of rotation of the Gaussian image relative to the object ($\chi = 0$ for pure electric lenses),

\mathcal{M} be the magnification of the lens defined by $R_I = \mathcal{M} R_p$

The eight aberrations may then be described as follows:

1) Distortion

$$\Delta R = S_1 R_p^3$$

2) Anisotropic distortion

$$R_I \Delta \theta = -S_2 R_p^3$$

3) Curvature of field

$$\Delta R = S_3 R_p^2 R_A \sin \psi$$

$$R_I \Delta \theta = S_3 R_p^2 R_A \cos \psi$$

4) Astigmatism

$$\Delta R = S_4 R_P^2 R_A \sin \psi$$

$$R_I \Delta \theta = -S_4 R_P^2 R_A \cos \psi$$

5) Anisotropic astigmatism

$$\Delta R = -S_5 R_P^2 R_A \cos \psi$$

$$R_I \Delta \theta = -S_5 R_P^2 R_A \sin \psi$$

6) Coma

$$\Delta R = S_6 R_P R_A^2 (2 - \cos 2\psi)$$

$$R_I \Delta \theta = S_6 R_P R_A^2 \sin 2\psi$$

7) Anisotropic coma

$$\Delta R = -S_7 R_P R_A^2 \sin 2\psi$$

$$R_I \Delta \theta = -S_7 R_P R_A^2 (2 - \cos 2\psi)$$

8) Spherical aberration or aperture defect

$$\Delta R = S_8 R_A^3 \sin \psi$$

$$R_I \Delta \theta = S_8 R_A^3 \cos \psi$$

When the source and the diffraction pattern are symmetric about the axis, it is necessary to consider only the radial component ΔR of the aberration figure. The angle ψ of the ray intersection in the aperture plane may be eliminated if the aberration figures are grouped by powers of R_A and R_P and described by the average value and the half width of ΔR .

Distortions:

$$\overline{\Delta R} = S_1 R_P^3 = S_1 \eta^3 R_I^3$$

$$\Delta R_{\frac{1}{2}} = 0$$

Field aberrations (curvature of field and astigmatism):

The image defect in the Gaussian image plane is

$$\Delta R = [(S_3 - S_4) \sin \psi - S_5 \cos \psi] R_P^2 R_A$$

then $\overline{\Delta R} = 0$,

$$\Delta R_{\frac{1}{2}} = \sqrt{(s_3 + s_4)^2 + s_5^2} (R_{PA}^2)$$

However, there is a surface where the ΔR component of the combination of curvature of field and isotropic astigmatism disappears. This is known as the tangential surface and is located at

$$(s_3 + s_4)(I - A)R_I^2 = (s_3 + s_4)(I - A)R_P^2$$

where $(I - A)$ is the distance from the aperture plane to the Gaussian image plane. The spreading of the image due to other aberrations is not greatly different at this surface than at the Gaussian image plane.

If the recording device is located at the tangential surface,

$$\Delta R_{\frac{1}{2}} \approx s_5 R_{PA}^2$$

Comas:

At the Gaussian image plane

$$\Delta R = [s_6(2 - \cos 2\psi) + s_7 \sin 2\psi] R_{PA}^2$$

This image defect is unsymmetrical

$$\overline{\Delta R} = 2s_6 R_{PA}^2$$

and

$$\Delta R_{\frac{1}{2}} = [2s_6 - \sqrt{s_6^2 + s_7^2}] R_{PA}^2$$

Spherical aberration, aperture defect:

At the Gaussian image plane

$$\Delta R = s_8 R_A^3 \sin \psi$$

$$\overline{\Delta R} = 0$$

$$\Delta R_{\frac{1}{2}} = s_8 R_A^3$$

It must be pointed out that aberration coefficients s_n are not constant for a given lens but depend on the focal length and the object and image

distances. However, for magnification greatly different from unity it is frequently assumed that S/n is constant for a given lens and focal length.

Chromatic aberrations. The chromatic aberrations fall into three groups:

1) Chromatic difference in magnification:

$$\Delta R = C_1 R_I P$$

$$R_I \Delta \theta = 0$$

2) Chromatic difference in rotation:

$$\Delta R = 0$$

$$R_I \Delta \theta = C_2 R_P$$

3) Chromatic difference in image position:

$$\Delta R = C_3 R_I \sin \psi$$

$$R_I \Delta \theta = C_3 R_I \cos \psi$$

C_2 is zero for a pure electric lens. Considering only the radial component ΔR and eliminating ψ as in the case of the geometric aberrations, the chromatic aberrations may be described by

Chromatic difference in magnification:

$$\overline{\Delta R} = C_1 R_P$$

$$\Delta R_{\frac{1}{2}} = 0$$

Chromatic difference in image position:

$$\overline{\Delta R} = 0$$

$$\Delta R_{\frac{1}{2}} = C_3 R_I$$

All of the chromatic aberration coefficients are proportional to the energy differences $e \Delta E$ of the electrons. The coefficient C_3 is always positive and never vanishes. Further, C_3 has an upper limit

$$C_3 < \left| \frac{\hbar \Delta E}{R_{\alpha} \Delta E} \right| R_m \left(1 + \frac{1}{|\eta|} \right)$$

where $R_{\alpha A}$ is the coordinate at the aperture plane, and R_m is the maximum value of an electron ray path which passes through the object at the axis with unit slope. As in the case of the geometric aberration coefficients, the chromatic aberration coefficients are functions of the focal length and of the object and image distances.

Space charge effects. Since electrons are charged particles, the field acting on the electrons will be different from those produced by the electrodes and polepieces of the lens. The electrons repel each other and the ray paths deviate from those predicted in the absence of space charge. The effect of space charge can be counteracted by modification of the lens design, but this correction can be made only for each particular distribution of electrons in the field. Fortunately, the space charge effects are of importance only when the electron density is high as it is in the electron gun and at the image of the source produced by the undiffracted electrons. For these reasons the space charge effects can be neglected in the design of a camera except in the electron gun which produces the effective electron source.

Collimating lens. When an electron lens is used to collimate the incident beam, an image of the source with its aberrations will be located at P in Figure 3. The diffraction pattern will be described by the same equations as in the case of the pinhole camera in which the size of the source is

$$R_P = \eta R_{Po} + \frac{S_8 R_A^3}{8} \quad (53)$$

neglecting all aberrations but spherical aberration*. The magnification η

* The complete expression is

$$R_P = \eta R_{Po} + S_1 R_{Po}^3 + \sqrt{(S_3 + S_4)^2 + S_5^2} (R_{Po}^2 R_A) + \left| 2 S_6 - \sqrt{S_6^2 + S_7^2} \right| R_{Po} R_A^2 + S_8 R_A^3 + C_1 R_{Po} + C_3 R_A$$

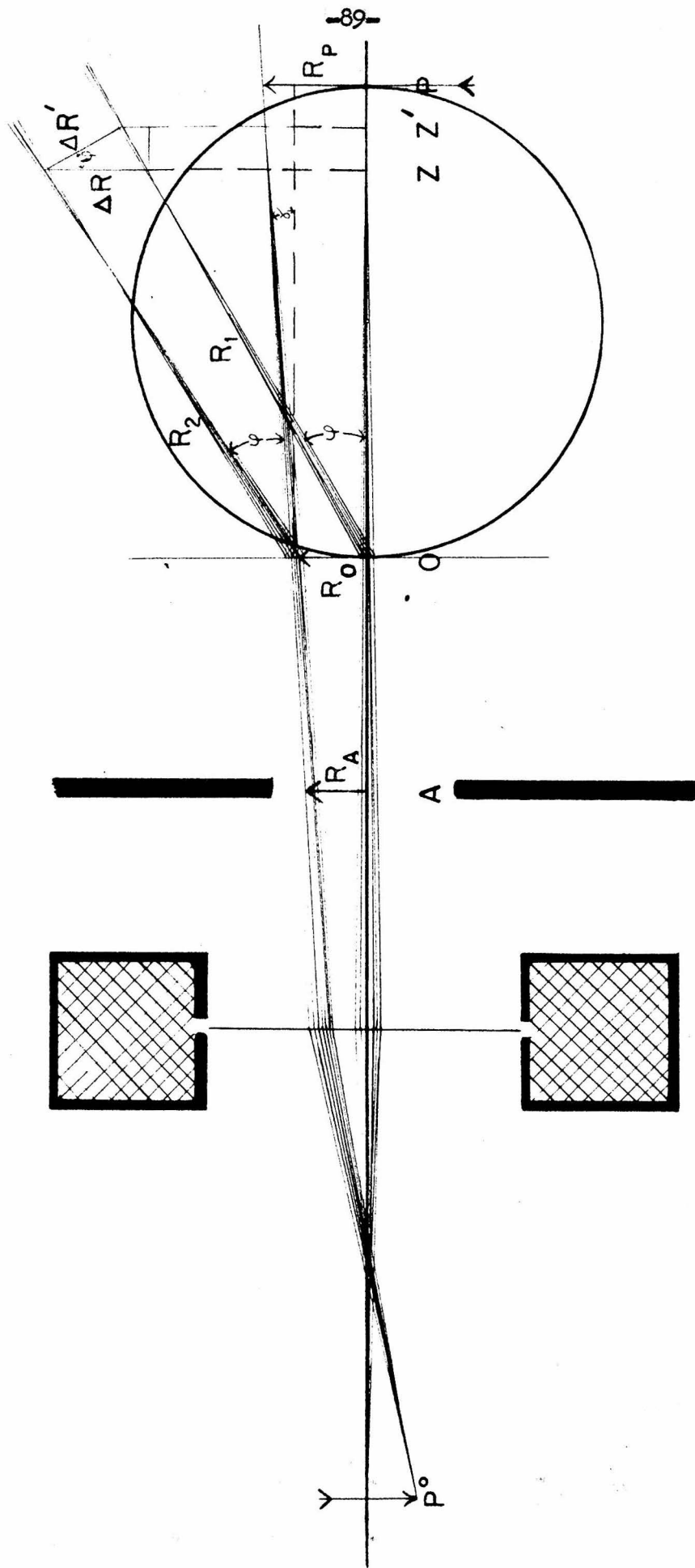


Figure 3

is the ratio of the distances from the principal plane of the lens to the image and to the source. The recording plane is now located in the opposite direction from the diffraction center than in the case of the pin-hole camera. The recording surface may now be located at $Z' = P \cos^2 \theta$ so that the "defocusing" term $(Z' \sec^2 \theta - P)R_{\lambda} / (P - A)Z \delta \sec^2 \theta$ in Equation (49) disappears.

Projector lens. An electron lens placed between the diffraction zone and the recording surface will focus the virtual diffraction pattern as shown in Figure 4. Let the virtual diffraction pattern described by Equation (49) lie on the surface (R_U, U) , where $Z' = U = P \cos^2 \theta$. An image of this pattern then is focused on the surface (R_V, V) . The object distance u from the principal plane of the lens is

$$u = U - H = P \cos^2 \theta - H,$$

where H is the principal plane. The image distance v from the principal plane is

$$V - H = v = \tau u = \tau (P \cos^2 \theta - H)$$

since the magnification of the lens is $\tau = v/u$. The magnification of the lens can be expressed in terms of the object distance u and the focal length $f = H - F$ by means of the lens equation, $1/f = 1/u + 1/v$; giving

$$\tau = f/(u - f) = (H - F)/(P \cos^2 \theta - F).$$

Then
$$v = (H - F)(P \cos^2 \theta - H)/(P \cos^2 \theta - F).$$

Let the image surface be defined by the parameters $\Delta Z_V = V(\theta) - V(\theta = 0)$

and the distance of the corresponding image point from the axis $R_V = \tau R_U$,

then
$$\Delta Z_V = -P(F - H)^2 \sin^2 \theta / (P - F)(P \cos^2 \theta - F) \tag{54}$$

and
$$R_V = \tau (P/2) \sin^2 \theta = (H - F)P \sin \theta \cos \theta / (P \cos^2 \theta - F).$$

When the diffraction center is located at the focus of the lens $F = 0$ and

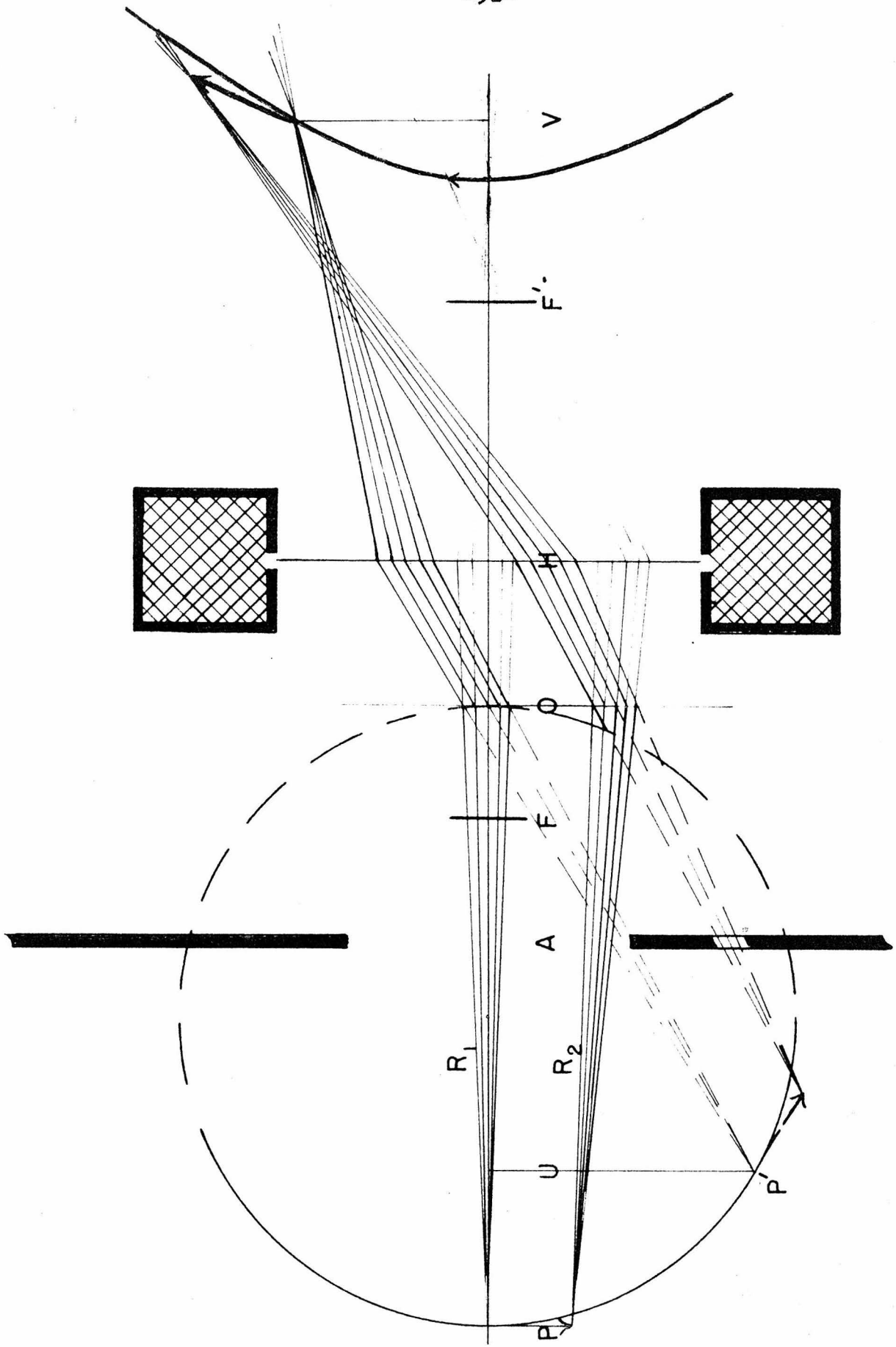


Figure 4

ΔZ_V and R_V simplify to

$$\Delta Z_V = -H^2 \tan^2 \phi / P \quad (54a)$$

and

$$R_V = H \tan \phi \quad (54a)$$

which may be combined to give

$$\Delta Z_V = -R_V^2 / P, \text{ a parabola} \quad (54b)$$

It is seen that as $P \rightarrow -\infty$ the image surface is a plane provided that F and H are not moved.

The effect of aberrations can be most readily treated if they are referred back to the virtual source. The image with its aberrations is passed back to the source through an ideal lens whose principal points are identical with the practical lens. Thus, the aberration seen at the virtual source is

$$\Delta R_U = \Delta R_V / m.$$

The aberration measured in $\Delta \phi$ from the diffraction center is approximately

$$\begin{aligned} \Delta \phi &\approx \tan \Delta \phi = \Delta R_U / P = \Delta R_V / m P \\ &= [\Delta R_V / (H - F)] [\cos^2 \phi - (F/P)]. \end{aligned} \quad (55)$$

In evaluating ΔR_V , $R_P = R_U = P \sin \phi \cos \phi$.

For distortion we find

$$\Delta \phi \approx [S_1 P^3 \sin^3 \phi \cos^3 \phi / (H - F)] (\cos^2 \phi - F/P).$$

It appears that $\tan \Delta \phi \rightarrow \infty$ as $P \rightarrow \infty$; however, $S_1 \rightarrow 0$ so that $\tan \Delta \phi$ remains finite. In electron microscopy S_n / h has been evaluated for large magnifications, the inverse of the above situation. This quantity is nearly constant for large magnification. If the object and image are reversed, the relation between the aberration coefficients, S_n for the forward process and S_n' for the reverse, is approximately

$$m \frac{S_n'}{m'} = S_n \quad (56)$$

$$m^{m-1} (S_n'/m') = S_n$$

where $m = 4$ for $n = 1, 2$
 $= 3$ for $n = 3, 4, 5$
 $= 2$ for $n = 6, 7$
 $= 1$ for $n = 8$

and where m is the magnification in the forward direction,

m' is the magnification in the reverse direction,

$$m m' = 1 \text{ e.}$$

This is equivalent to imaging the virtual source through an ideal lens and referring the image back to the source through the practical lens.

Hence, for the various aberration $\Delta \phi$ may be expressed in terms of S_n , the forward aberration coefficient, or S_n' , the backward aberration coefficient.

Distortion.

$$\overline{\Delta \phi} = (S_1/m) P^2 \sin^3 \phi \cos^3 \phi \quad (57a)$$

$$\overline{\Delta \phi} = (S_1'/m') \left(\frac{H-F}{1 - (F/P) \sec^2 \phi} \right)^2 \tan \phi \sin^2 \phi$$

This is the displacement of the diffraction. The effect on resolution depends on the size of the virtual source. It is given approximately by

$$\Delta \phi_{\frac{1}{2}} \approx (S_1'/m') \left(\frac{H-F}{1 - (F/P) \sec^2 \phi} \right) \tan \phi \sin \phi (2 \cos \phi \sin \delta \phi) \quad (57b)$$

where $\delta \phi$, the angle subtended by the source at the diffraction center, is small.

Field aberrations. The best image is obtained when the image

surface coincides with the tangential surface of the lens. This surface will be given by

$$\begin{aligned}\Delta z_T &\approx (s_3 + s_4)wR_U^2 + \Delta z_V \\ &\approx [(s_3 + s_4)/m] wR_U^2 + \Delta z_V\end{aligned}$$

or

$$\Delta z_T \approx [(s_3' + s_4')/m'] wR_U^2 + \Delta z_V \quad (58)$$

On this surface one finds:

$$\Delta \phi = (s_5/m)R_A P \sin^2 \phi \cos^2 \phi \quad (59)$$

or

$$\Delta \phi = (s_5'/m')R_A [(H - F)/(1 - F/P)] \sin^2 \phi$$

Coma and anisotropic coma.

$$\Delta \phi = s_6/m \left[2 + \sqrt{1 + (s_7/s_6)^2} \right] R_A^2 \sin \phi \cos \phi \quad (60)$$

or

$$\Delta \phi = s_6'/m' \left[2 + \sqrt{1 + (s_7/s_6)^2} \right] R_A^2 \sin \phi \cos \phi$$

Spherical aberration, aperture defect.

$$\Delta \phi = (s_8/m)(R_A^3/P) \quad (61)$$

or

$$\Delta \phi = (s_8'/m')(R_A^3/H - F)(\cos^2 \phi - F/P)$$

Chromatic difference in magnification.

$$\Delta \phi = (C_1/m) \sin \phi \cos \phi \quad (62)$$

or

$$\Delta \phi = (C_1'/m') \sin \phi \cos \phi$$

Chromatic difference in image position.

$$\Delta \phi = (C_3/m)(R_A/P) \quad (63)$$

or

$$\Delta \phi = (C_3'/m')(R_A/H - F)(\cos^2 \phi - F/P)$$

More than one electron lens. Some advantages may be obtained by the use of both a collimating and a projector lens. Such a system is illustrated in Figure 5. The collimating lens focuses a virtual image at P of a source at P^0 . After diffraction a virtual scattering pattern described in terms of P , O , H , and F is focused by the projector lens at V . Such a combination of lenses permits the construction of a camera of limited dimensions with an effective source at any distance. Inspection of Equations (54) will show that the shape of the image surface is much simpler when the effective source is at infinity. The virtual diffraction pattern is described by Equations (49), (51), and (52), the aberrations of the collimating lens by Equation (53), and those of the projector lens by Equations (57) to (63).

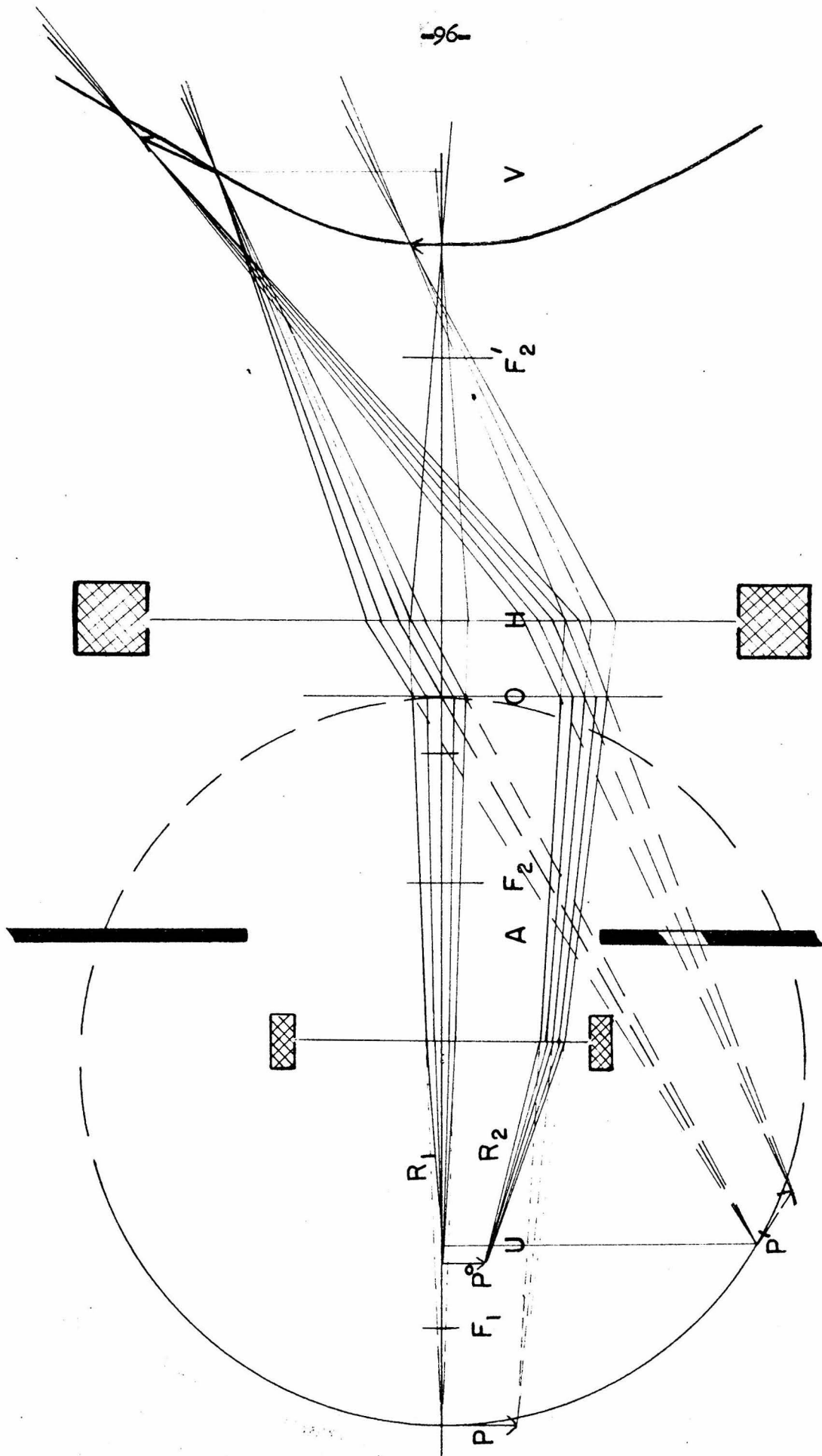


Figure 5

MULTIPLE SCATTERING

The effect of multiple scattering on the diffraction pattern is readily discussed if this occurrence is treated as a kind of spreading. Consider separately the patterns that would be obtained if all the electrons were scattered not at all, once, twice, and so forth. The observed diffraction pattern then may be visualized as the superposition of these separate patterns. That is

$$I_M(s) = \psi_0^{(0)} I(s) + \psi_1^{(1)} I(s) + \psi_2^{(2)} I(s) + \dots \quad (64)$$

where ψ_m is the probability of an electron being scattered m times and $^{(m)}I(s)$ describes the angular distribution of electrons scattered m times.

Estimation of scattering probabilities. Let $\bar{\mu}$ be the mean probability of scattering an electron, then

$$\bar{\mu} = \frac{N \int_{j_1} \int_0^{4\pi} I(s) d\omega}{A \int_{j_1}} = n \sigma l \quad (65)$$

where $\sigma = \int_0^{4\pi} I(s) d\omega$ is called the scattering cross-section of the molecules for electrons.

Assume that all the effective electron paths in diffraction volume are identical, then the increment of ψ_m in the distance dl is

$$d\psi_m = -n\sigma [\psi_{m-1} - \psi_m] dl \quad (66)$$

and
$$\psi_m = \exp(-n\sigma l) \left[\int \psi_{m-1} \exp(n\sigma l) n\sigma dl + C \right] \quad (67)$$

Evaluating (67) for $m = 0, 1, 2, \dots$ with the conditions $\psi_{-1} = 0$, $\psi_0(0) = 1$ and $\psi_{m>1}(0) = 0$ it is found that

$$\psi_m(\bar{1}) = \frac{(n\sigma\bar{1})^m \exp(-n\sigma\bar{1})}{m!} = \frac{\bar{\mu}^m \exp(-\bar{\mu})}{m!} \quad (68)$$

This distribution of the probability of multiple events is known as the Poisson distribution.

Fourier transforms of m-tuple scattering functions in two dimensions.

The scattering function for no scattering may be represented by the δ -function $\delta(s)$. The scattering function for single scattering is, of course, $Q(s)$. In the case of double scattering the diffraction pattern is spread about each point of a single scattering function. It is equivalent to say that the double scattering function is the single scattering function folded with itself in two dimensions.

$${}^{(2)}Q(x,y) = \int_{-\infty}^{\infty} \int_{-\infty}^{\infty} {}^{(1)}Q(u,w) {}^{(1)}Q(x-u, y-w) du dw \quad (69a)$$

where $x = s \cos \theta$, $y = s \sin \theta$, $u = t \cos \theta'$, and $w = t \sin \theta'$. For m-tuple scattering it will be seen by induction that

$${}^{(m)}Q(x,y) = \int_{-\infty}^{\infty} \int_{-\infty}^{\infty} {}^{(m-1)}Q(u,w) {}^{(1)}Q(x-u, y-w) du dw \quad (69b)$$

The two-dimensional Fourier transform $\Delta(\xi, \eta)$ of $Q(x,y)$ is defined by

$$\Delta(\xi, \eta) = (1/2\pi) \int_{-\infty}^{\infty} \int_{-\infty}^{\infty} Q(x,y) \exp i(\xi x + \eta y) dx dy \quad (70)$$

It can then be shown that

$${}^{(0)}\Delta(\xi, \eta) = 1$$

and

$${}^{(m)}\Delta(\xi, \eta) = {}^{(m-1)}\Delta \cdot {}^{(1)}\Delta = {}^{(1)}\Delta^m(\xi, \eta). \quad (71)$$

Combining Equations (64), (68), and (71), the two-dimensional transform

Δ_m of the multiple scattering function is

$$\Delta_M(\xi, \eta) = \exp(-\bar{\mu}) \sum_{m=0}^{\infty} \frac{\bar{\mu}^m (1) \Delta_m}{m!} \quad (72)$$

$$\Delta_M(\xi, \eta) = \exp(-\bar{\mu}) \exp(\bar{\mu} (1) \Delta) = \exp \bar{\mu} ((1) \Delta - (0) \Delta) .$$

Relation between the one and two dimensional Fourier transforms.

When $\mathcal{Q}(x,y)$ is radially symmetric, i.e. $\mathcal{Q}(x,y) = \mathcal{Q}(s)$, it is appropriate to transform Equation (70) to polar coordinates by the substitutions:

$$x = s \cos \theta, \quad y = s \sin \theta, \quad \xi = \rho \cos \zeta, \quad \eta = \rho \sin \zeta$$

$$\Delta(\rho, \zeta) = (1/2\pi) \int_0^{\infty} \int_0^{2\pi} s \mathcal{Q}(s) \exp[i \rho s \cos(\theta - \zeta)] d\theta ds \quad (73)$$

which may be written:

$$\Delta(\rho) = \int_0^{\infty} s \mathcal{Q}(s) J_0(\rho s) ds \quad (74)$$

where $J_0(\rho s)$ is the zeroth order Bessel function of the first kind. The one-dimensional transform is

$$\mathcal{D}(r) = (1/\sqrt{2\pi}) \int_{-\infty}^{\infty} \mathcal{Q}(s) \exp(i r s) ds \quad (75)$$

$\mathcal{Q}(s)$ is related to both the one and two dimensional transforms by the Fourier inversion theorem:

$$s \mathcal{Q}(s) = (-1/\sqrt{2\pi}) \int_{-\infty}^{\infty} \frac{\partial \mathcal{D}(r)}{\partial r} \exp(-i r s) ds \quad (76)$$

and

$$\mathcal{Q}(s) = \int_0^{\infty} \rho \Delta(\rho) J_0(\rho s) d\rho \quad (77)$$

Substituting Equation (76) in Equation (74)

$$\Delta(\rho) = -(1/\sqrt{2\pi}) \int_{-\infty}^{\infty} \frac{\partial \mathcal{D}(r)}{\partial r} \int_0^{\infty} i J_0(\rho s) \exp(-i r s) ds dr \quad (78a)$$

$$\Delta(\rho) = - (1/\sqrt{2\pi}) \int_{-\infty}^{\infty} \frac{\partial D(r)}{\partial r} \int_0^{\infty} J_0(\rho s) \sin rs \, ds \, dr \quad * \quad (78b)$$

$$\int_0^{\infty} J_0(\rho s) \sin rs \, ds = \begin{cases} 0 & , r < \rho \\ \infty & , r = \rho \\ \frac{1}{r\sqrt{1-\rho^2/r^2}} & , r > \rho \end{cases} \quad \delta$$

and
$$\Delta(\rho) = -\sqrt{2/\pi} \int_{\rho}^{\infty} \frac{\partial D(r)}{\partial r} \frac{dr}{\sqrt{r^2-\rho^2}} \quad , \rho \neq 0 \quad (78c)$$

Substituting Equation (77) in Equation (75)

$$D(r) = (1/\sqrt{2\pi}) \int_0^{\infty} \rho \Delta(\rho) \int_{-\infty}^{\infty} J_0(\rho s) \exp(i rs) \, ds \, d\rho \quad (79a)$$

$$D(r) = \sqrt{2/\pi} \int_0^{\infty} \rho \Delta(\rho) \begin{cases} 0 & , \rho < r \\ \infty & , \rho = r \\ \frac{1}{\sqrt{\rho^2-r^2}} & , \rho > r \end{cases} d\rho \quad (79b)$$

$$D(r) = \sqrt{2/\pi} \int_r^{\infty} \frac{\rho \Delta(\rho)}{\sqrt{\rho^2-r^2}} d\rho \quad , r \neq 0 \quad (79c)$$

The one-dimensional Fourier transform of the multiple scattering

function. The interpretation of the one-dimensional Fourier transform of the scattering function is familiar and readily understood. Combining

*
$$\int_{-\infty}^{\infty} \frac{\partial D(r)}{\partial r} \int_0^{\infty} J_0(\rho s) \cos rs \, ds \, dr = 0 \quad , \text{ since the}$$

integrand
$$\frac{\partial D(r)}{\partial r} \int_0^{\infty} J_0(\rho s) \cos rs \, ds$$
 is odd.

Equations (72), (78) and (79) the one-dimensional transform of the multiple scattering function is:

$$D_M(r) = \sqrt{\frac{2}{\pi}} \int_r^\infty \left\{ \exp(-\mu) \left[1 + \sqrt{\frac{2}{\pi}} \int_e^\infty \frac{\partial^{(1)} D(p)}{\partial p} \frac{dp}{\sqrt{p^2 - e^2}} \right] \right\} \frac{e \partial e}{\sqrt{e^2 - r^2}} \quad (80)$$

An alternate expression can be derived by combining Equations (64) and (68) with (79c)

$$D_M(r) = \sqrt{2/\pi} \left\{ 1 + \sum_{m=1}^{\infty} \frac{\mu^m \exp(-\mu)}{m!} \int_r^\infty \frac{e^{(1)m}(e)}{\sqrt{e^2 - r^2}} de \right\}, \quad r \neq 0 \quad (81)$$

and

$$D_M(r) = \sqrt{2/\pi} \left\{ 1 + \sum_{m=1}^{\infty} \frac{\mu^m \exp(-\mu)}{m!} \int_r^\infty \left(\int_e^\infty \frac{\partial^{(1)m} D(p)}{\partial p} \frac{dp}{\sqrt{p^2 - e^2}} \right) \frac{e de}{\sqrt{e^2 - r^2}} \right\}$$

There has not been time to carry these expressions further so that their meaning would be clarified. Several approximations can be examined and qualitative interpretations made.

The effect of folding the function $a + b(\sin rs)/rs$ with itself in one and in two dimensions may be compared qualitatively. In one dimension, the folded function becomes $c + d(\sin rs)/rs$ where $d/c \ll b/a$. In two dimensions the folded function becomes more like a zeroth order Bessel function plus a constant; that is, the zeros of the varying component are no longer equally spaced and the amplitude does not fall off as fast as $1/s$. Both kinds of folding show that the ratio of the amplitude of the periodic component to the constant component is reduced. In addition, the two-dimensional folding, which represents the physical picture, shifts the central maxima and minima inward, corresponding to longer apparent

distances, and the amplitude of the outer part of the function is not reduced as rapidly as in the case of one-dimensional folding.

With these differences in mind better approximations to the intensity function may be examined by one-dimensional folding. First, it is found that when there is more than one distance in a molecule the longest distances are erased more rapidly than the shorter ones. Second, the apparent distances are shortened; this shortening is compensated in part by the apparent lengthening found in the two-dimensional case.

Of all the effects of multiple scattering the increase of the ratio of background (atomic and incoherent scattering) to the molecular scattering is the most important.

THEORETICAL LIMITATIONS OF ELECTRICAL RECORDING

Workers in the field of electron diffraction have sought mechanical methods of obtaining data. Densitometry of films has been used to some extent. Direct measurement of the scattered electrons has been suggested, but at present no practical method applicable to gases has appeared. It is possible, however, to estimate the theoretical limit of the performance of a hypothetical but partly idealized system. No practical system can exceed this limit.

The hypothetical system. Let the source and recording surface be placed infinitely far from the diffraction zone which has a finite length \bar{l} and cross-section \bar{C} . The only uncertainties in the scattering angle are those arising from the finite angles subtended to the diffraction center by the source and by the recording element and those due to any lens aberrations. The lens aberrations will be neglected.

For a practical example the cross-section of the scattering zone will be $\bar{C} = 1 \text{ mm.}^2 = 10^{-2} \text{ cm.}^2$ and the mean probability of scattering, $\bar{\mu} = 0.1$. The cathode will be operated at $\sim 2600^\circ\text{K}$; so that the specific emissivity is 1 amp./cm.^2 . An accelerating potential of forty kilovolts and a wavelength of 0.06 \AA . will be used. An exposure time of $t = 0.1$ sec. is reasonable.

The limit of observation. The limit of observation s_m has been given by Equation (23) which at large scattering angles is approximately

$$s_m^5 = K_1 j_i |\Theta| \Delta\omega/j_0 (1 + eE/kT) r_{ij} \Delta Q_{\min} \quad (82)$$

where $K_1 = K^2 Z_i Z_j \overline{nICtj_0} (1 + eE/kT) = 282 Z_i Z_j / \sigma_m$. Substituting from Equations (25), (34), and (42)

$$s_m^4 = K_1 \sin^2 \alpha \exp(-\sum w_{ij}^2 / 6) (\lambda / 2\pi)^2 \Delta s_r \Delta \theta_r / r_{ij} \Delta Q_{\min} \quad (83)$$

where α is the half-angle subtended by the source and Δs_r is the width of the angle $\Delta \theta_r$ subtended by a recording element. If w_p is the half-width of the source and w_r the half-width of the recording element, then

$$w_p = 4\pi/\lambda \cos(\theta/2) \sin \alpha / 2 \approx (2\pi/\lambda) \sin \alpha$$

$$w_r = \Delta s_r / 2$$

and

$$s_m^4 = 2K_1 (\lambda / 2\pi)^4 w_r w_p^2 \exp[-(w_r^2 + w_p^2) r_{ij}^2 / 6] \Delta \theta_r / r_{ij} \Delta Q \quad (84)$$

If the recording elements are equal segments of annuli, then $\Delta \theta_r$ is constant. Let either $w_r w_p^2$ or $w_r^2 + w_p^2$ be held constant, then s_m will be a maximum when $w_r^2 = 2w_p^2$ and

$$s_m^4 = 4K_1 (\lambda / 2\pi)^4 w_r^3 \exp(-w_r^2 r_{ij}^2 / 2) \Delta \theta_r / r_{ij} \Delta Q \quad (85)$$

In the case where the recording element is approximately square,

$$\Delta \theta_r = \Delta s_r / s_r = 2w_r / s_r \text{ and}$$

$$s_m^5 = 4K_1 (\lambda / 2\pi)^4 w_r w_p^2 \exp[-(w_r^2 + w_p^2) r_{ij}^2 / 6] / r_{ij} \Delta Q \quad (86)$$

which is a maximum, holding $w_r w_p^2$ or $w_r^2 + w_p^2$ constant when $w_r^2 = w_p^2$. So

that

$$s_m^5 = 4K_1 (\lambda / 2\pi)^4 w_r^4 \exp(-w_r^2 r_{ij}^2 / 3) / r_{ij} \Delta Q \quad (87)$$

The limit of detection of a distance. The exponential function in these Equations (from Equation (34)) describes the change of detect-

ability with the length of the interatomic distance. Since there is no practical optimum value* for w_r in the exponential, w_r will be determined by giving the exponential the arbitrary value $\sqrt{2}$ when r_{ij} equals the longest distance to be measured. The widths w_r in Equations (85) and (87) are then $0.83/r_{ij}^1$ and $1.026/r_{ij}^1$ respectively, where r_{ij}^1 is the longest distance to be observed.

$$s_m^4 = 1.61 K_1 (\lambda/2\pi)^4 \Delta \theta_r / r_{ij}^3 r_{ij} \Delta Q_{\min} \quad (88a)$$

and

$$s_m^5 = 3.02 K_1 (\lambda/2\pi)^4 / r_{ij}^4 r_{ij} \Delta Q_{\min} \quad (88b)$$

The sensitivity. Equations (88) represent for the case of a rigid diatomic molecule twice the difference in the charges scattered at a maximum and at a minimum. The limit of observation is the point where the presence of a maximum or a minimum is just detectable. If Equations (88) are multiplied by a factor of two, the maximum uncertainty in the measurement of the scattered charge necessary to observe a distance r_{ij} out to s_m will be found to be

$$\Delta Q_{\min} = 3.22 K_1 (\lambda/2\pi)^4 \Delta \theta_r / r_{ij}^3 r_{ij} s_m^4 \quad (89a)$$

$$\Delta Q_{\min} = 4.76 \times 10^{-5} (z_i z_j / \sigma) / r_{ij}^3 r_{ij} s_m^4$$

($\Delta \theta_r = 2\pi$)

and

$$\Delta Q_{\min} = 3.02 K_1 (\lambda/2\pi)^4 / r_{ij}^4 r_{ij} s_m^5 \quad (89b)$$

$$\Delta Q_{\min} = 1.42 \times 10^{-5} (z_i z_j / \sigma) / r_{ij}^4 r_{ij} s_m^5$$

* Maximizing Equations (85) and (87) with respect to the width leads to $w_r = 3/r_{ij}$ and $6/r_{ij}$, and the values of the exponential become 0.22 and 0.14, respectively. If w_r is selected for the longest distance in the molecules, the difference in the relative detectability of the longest and shortest distances would be intolerable.

The longest detectable distance using the camera in this laboratory is probably $r_{ij}^0 \approx 5 \text{ \AA}$. Professor Schomaker states that the molecular pattern of ethane is scarcely observable at $s = 30$. The amplitude of the molecular component of the pattern is reduced to about 0.2 by the temperature factor. $Z_i Z_j / s$ is approximately 3.6 and the interatomic distance is $r_{ij} = 1.54$ for this molecule. Hence, to equal the performance the uncertainty in the measurement of the charge must be less than

$$\Delta Q_{\min} = 3.76 \times 10^{-13} \text{ coulombs}$$

when the recording elements are annular, and

$$\Delta Q_{\min} = 6.88 \times 10^{-16} \text{ coulombs}$$

when the recording elements are approximately square. If allowance is made for the idealization in this calculation, the sensitivity of measurement in the two cases will have to be of the order of magnitude of 10^{-14} to 10^{-15} and 10^{-17} respectively.

Appendix I

Fourier transform of spreading functions of the second class.

The integral

$$D_0(r) = (1/\sqrt{2\pi}) \int_{-\infty}^{\infty} \int_{-\infty}^{\infty} \frac{Q(t)}{t} G_{II} \left(\frac{s-t}{t} \right) \exp(irs) dt ds \quad (i)$$

is to be evaluated. This integral can be written

$$D_0(r) = (1/\sqrt{2\pi}) \int_{-\infty}^{\infty} \int_{-\infty}^{\infty} Q(t) \exp(irt) \frac{1}{t} G_{II} \left(\frac{ss-t}{t} \right) \exp[ir(ss-t)] dt ds.$$

Making the substitution $u = ss - t$ and inverting the order of integration leads to

$$D_0(r) = \int_{-\infty}^{\infty} Q(t) G_{II}(rt) \exp(irt) dt \quad (ii)$$

By the Fourier inversion theorem

$$Q(t) = (1/\sqrt{2\pi}) \int_{-\infty}^{\infty} D(p) \exp(-ipt) dp, \quad (iii)$$

hence $D_0(r) = (1/\sqrt{2\pi}) \int_{-\infty}^{\infty} \int_{-\infty}^{\infty} D(p) G_{II}(rt) \exp[-i(p-r)t] dp dt, (iv)$

which gives

$$D_0(r) = \int_{-\infty}^{\infty} [D(p)/r] G_{II} [(p-r)/r] dp \quad (v)$$

References

1. Brockway, L. O., Rev. Mod. Phys., 8, 231 (1936)
2. Bewilogua, L., Physik. Zeits., 32, 740 (1931)
3. Wierl, R., Ann. Phys., 8, 521 (1931)
4. Langmuir, D. B., Proc. Inst. Radio Engrs., 25, 977 (1937)
5. Richardson, O. W., Emission of Electricity from Hot Bodies, rev. ed., Longmans, Green & Company, New York, (1921)
Dushman, S., Phys. Rev., 21, 623 (1923)
6. Glaser, W., Z. Physik., 83, 104 (1933)
Schezzer, O., Z. Physik., 101, 593 (1936)
Rogowski, W., Arch. Elektrotech., 31, 555 (1937)
7. Zworykin, V. K., Electron Optics and the Electron Microscope, 1st ed., John Wiley & Sons, Inc., New York (1945) Chapter 16
8. Watson, G. N., Treatise on the Theory of Bessel Functions, 1st ed., Cambridge (Eng.), The University Press (1922) p. 405

PROPOSITIONS

1. The standard entropy reported for formic acid¹ includes $\frac{1}{2} R \ln 2$ e.u. as suggested by Pauling² for the randomness at absolute zero of the positions of the hydrogen atoms in the hydrogen bonds of the dimer. An interpretation of the transition found in sebacic acid (this thesis) indicates that the hydrogens are oriented in this crystal and suggests that the randomness in other carboxylic acids may not be "frozen in". I propose that the calculation³ of the entropy of formic acid monomer from spectroscopic data be reinvestigated.

2. The measurement of Soret coefficients is notable for the lack of agreement among various observers. It is most likely that these disagreements arise from the failure to completely suppress all convection currents. I propose that thermal diffusion cells be constructed using a porous diaphragm between two thermostated reservoirs. The pores of the diaphragm can be small enough that convection is negligible. The solutions should be circulated within each reservoir.

3. The recording surface in an electron diffraction camera can be shaped so that the measured ring diameters (or radii) are proportional to the scattering parameter $s = (4\pi/\lambda)\sin\theta/2$. If the electron wavelength is 0.06 \AA and if the distance from the scattering center to the surface along the undiffracted beam is L , then such a surface is approximated, out to $ss = 80$, within a few tenths of one percent by a sphere whose radius is $3L/4$.

4a. The synthesis of radial distribution functions in the analysis of electron diffraction data is becoming more extensive in this laboratory. Although the Gaussian cards prepared by A. Perlis⁴ have proved useful for such syntheses, cards designed particularly for this calculation would be more flexible. I suggest that cards tabulating the transform of the modification function be prepared for use with the "L" board. The function should be tabulated at 0.05 Å. intervals and the displacement ("frequency") either 0.01 or 0.02 Å. It is desirable that the function be tabulated for several widths and that the amplitude unit be defined in terms of a unit sine function.

4b. Interpolation polynomials are satisfactory approximations for many functions. The interpolation polynomial and its derivatives can be expressed as a linear combination of the ordinates. The coefficients for the first derivative have been tabulated for several groups of equally spaced points⁵ and should be placed on punched cards in this laboratory. The calculation of derivatives may be used in the analysis of electron diffraction data. In particular the modification functions $s^2 \exp(-as^2)$ and $s^4 \exp(-as^2)$ suggested by J. Waser and V. Schomaker are equivalent to

$$-k \frac{\partial^2}{\partial r^2} \int_{-\infty}^{\infty} \exp(-p^2/4a^2) (r-p) D(r-p) dp$$

$$k \frac{\partial^4}{\partial r^4} \int_{-\infty}^{\infty} \exp(-p^2/4a^2) (r-p) D(r-p) dp$$

where $rD(r)$ is the sine transform of $sI(s)$.

5. The Fourier synthesizer built by Pepinsky⁶ uses all-electronic wave

generators. I propose that electro-mechanical generators similar to the tone wheels in the Hammond electric organ would be more satisfactory when the range of this computer is extended beyond terms of the twentieth order.

6. Nuclear resonance measurements will be useful in settling the structure of diborane.

7. The approximation of a function with polynomials or with a power series by the method of least squares can be greatly simplified when the abscissae are equally spaced⁷. I believe that the labor in computing the coefficients of a power series is reduced in the case of randomly spaced abscissae if, first, the coefficients are obtained for a series of polynomials which are orthogonal with respect to sums at equally (or nearly equally) spaced points and, then, the series of polynomials is converted into a power series.

8 a. The amplitude of the zeroth ("central") maximum in visual curves is frequently estimated to be 1.3 times the average amplitude of the maxima and minima. This empirical rule can be rationalized leading to the approximate expression

$$\sqrt{2} \exp(-\sigma^2 s^2 / 2) \bar{A}$$

for the probable amplitude of the "central" maximum, where σ is the second moment (standard deviation) of the interatomic distances and \bar{A} is the root-mean-square amplitude of the visual curve. \bar{A} is given approximately by

$$\bar{A}^2 \approx \sum_i^n a_i^2 w_i / 2n \quad w_i \approx \sum_i^n a_i^2 / 2n$$

where a_i is the amplitude and w_i is the width of the i 'th maxima or minima. This approximation has several limitations.

8. b. The removal of part of the baseline error can be facilitated by inspection of the integral of the visual curve. The baseline of the integral is located approximately by an ordinate passing through the integral at the abscissas of the central (zeroth) maximum of the visual curve.

9. A large amount of incoherent scattering of electrons has been reported by some observers in iodine-containing compounds. I propose that part of this may arise from resonance between the incident electrons and the K electrons in the iodine atoms. Experiments should be made by varying the accelerating potential.

10. a. The intensity of the beam in the electron diffraction camera can be increased readily by increasing the size of the filament wire.

b. A spring shutter from an ordinary camera can be adapted to the electron diffraction camera and would enable exposures to be made more reproducibly than at present.

c. The state of the art of electronic voltage regulation is sufficiently advanced that a practical application can be made for electron diffraction.

d. A secondary wavelength standard can be built using two readily calibrated voltage dividers arranged in a Wheatstone bridge for comparison of the two dividers and would be more satisfactory than the present arrangement in this laboratory.

11. a. The propositions presented by candidates for the degree of

Doctor of Philosophy in this department should be collected in one place and made available to all graduate students

11. b. Each year the best propositions should be selected and published.

References

1. Stout, J.W. and Fisher, L.H., J. Chem. Phys., 9, 163 (1941)
2. Pauling, L., J. Am. Chem. Soc., 57, 2680 (1935)
3. Halford, J.O., J. Chem. Phys., 9, 859 (1941); 10, 582 (1942)
4. Perlis, A., Masters Thesis, California Institute of Technology (1947)
5. Table of Coefficients for Obtaining the First Derivative Without Differences, National Bureau of Standards, N.B.S., Applied Mathematics Series 2, U.S. Government Printing Office, Washington (1948)
6. Pepinsky, R., J. Applied Phys., 18, 601 (1947)
7. Milne, W.E., Numerical Calculus, mimeographed notes, Oregon State College (1941)
- Barge, R.T., Rev. Mod. Phys., 19, 298 (1947)